APPLICATION OF SIMUFACT IN SIMULATING THE ACTUAL MAXIMUM STRESS IN A TUNGSTEN INERT GAS WELDMENT

BY

ODOKARA EMMANUEL CHIBUZOR

ENG2006320

DEPARTMENT OF INDUSTRIAL ENGINEERING,

FACULTY OF ENGINEERING

UNIVERSITY OF BENIN, BENIN CITY.

SEPTEMBER, 2025

APPLICATION OF SIMUFACT IN SIMULATING THE ACTUAL MAXIMUM STRESS IN A TUNGSTEN INERT GAS WELDMENT

BY

ODOKARA EMMANUEL CHIBUZOR

ENG2006320

A RESEARCH PROJECT WRITTEN AND SUBMITTED TO THE DEPARTMENT OF INDUSTRIAL ENGINEERING, FACULTY OF ENGINEERING, UNIVERSITY OF BENIN, IN PARTIAL FULFILMENT OF THE REQUIREMENTS FOR DEGREE OF BACHELOR OF ENGINEERING OF THE UNIVERSITY OF BENIN, BENIN CITY

SEPTEMBER, 2025

DECLARATION

I declare that:

This project work is based on a study undertaken by me in the Department of Industrial Engineering, University of Benin under the supervision of Engr. Dr. B.O ERHUNMWUNSE. This work has not been previously submitted for award of a degree elsewhere.

All ideas and views are products of my personal research effort and all references to works of others has been duly acknowledged.

_____

ODOKARA EMMANUEL CHIBUZOR

DATE: _____

CERTIFICATION

We certify that ODOKARA EMMANUEL CHIBUZOR with the matriculation number ENG2006320 submitted the research work to the department of industrial engineering, Faculty of Engineering, University of Benin City.

_____ _____

Engr. Dr. B.O ERHUNMWUNSE DATE

Project supervisor

_____ _____

Engr Dr E.M. ETUK DATE

Project coordinator

_____ _____

Prof P.E. AMIOLEMHEN DATE

Head of department

DEDICATION

This project is dedicated to God Almighty, the source of wisdom and strength, whose guidance made this work possible. It is also dedicated to my parents and family for their unwavering love, support, and encouragement throughout my academic journey.

ACKNOWLEDGEMENTS

I wish to express my profound gratitude to God Almighty for His grace, guidance, and blessings that made the successful completion of this project possible.

My sincere appreciation goes to my supervisor, Engr. Dr. B.O ERHUNMWUNSE, for his mentorship, invaluable guidance, and patience throughout the course of this research. I am also grateful to all the lecturers and staff of the Department of Industrial Engineering, University of Benin**,** for imparting knowledge and providing the enabling environment for learning and research.

Special thanks go to my colleagues and friends for their cooperation and moral support. Lastly, I deeply appreciate my parents Mr. and Mrs. Odokara and family for their continuous prayers, motivation, and encouragement throughout this project.

ABSTRACT

This study investigates the simulation of the actual maximum stress in Tungsten Inert Gas (TIG) weldment using SIMUFACT Welding software. The research aimed to compare the simulated stress values with experimental results obtained in a controlled environment under varying process parameters such as current, voltage, and gas flow rate.

During the design of experiment, twenty experimental runs was generated by the Central composite design and it was used to carry out TIG welding on mild steel plates. A universal testing machine was used to record the actual maximum stress on the welded joint and recorded as experimental values. The data generated from the CCD matrix was then feed into an expert system (SIMUFACT 2024) which was used to carry out TIG welding simulations with its corresponding actual maximum stress recorded alongside as the SIMUFACT result.

Results from this study revealed that that increasing welding current reduces the maximum stress due to higher heat input and lower cooling rate, while voltage variation influences arc width and stress distribution. The actual maximum stress values from both datasets were analyzed and compared. The results revealed close agreement between experimental and simulated values, a fitted line plot was used to ascertain the degree of correlation between both results and a correlation coefficient of 0.98 was observed, indicating a very strong positive correlation degree between the experimental result and the **SIMUFACT** result. A time series plot was then used to compare if both data sets assumed the same trend. The SIMUFACT welding simulation analysis proved to be a reliable tool for simulating and predicting the actual maximum stress in TIG-welded joints thereby aiding in the optimization of welding parameters for an improved structural integrity

TABLE OF CONTENTS

LIST OF FIGURES

LIST OF TABLES

CHAPTER ONE

INTRODUCTION

1.1 Background to the study

Welding is a critical manufacturing process for joining metals and thermoplastics through fusion or solid-state bonding. Its applications span high-integrity industries such as aerospace, automotive, and pressure vessel fabrication, where joint reliability dictates structural performance (Kou, 2003; Pandey *et al*., 2021). Despite its advantages, welding introduces thermo-metallurgical alterations that degrade mechanical properties in the weld zone, often making it the epicenter of failure under operational stresses (Messler, 2008; Kumar, 2020). Welding techniques are primarily categorized into fusion welding and solid-state welding. solid-state welding methods includes friction stir welding and ultrasonic welding, these achieve bonding without melting, relying on mechanisms such as plastic deformation and atomic diffusion (Kalpakjian and Schmid, 2014; Messler, 2008), while on the other hand,

Fusion welding entails melting the base metals to form a joint through solidification of the molten pool. Common examples include Gas Metal Arc Welding (GMAW), Shielded Metal Arc Welding (SMAW), Submerged Arc Welding (SAW), and Tungsten Inert Gas (TIG) welding. However, each welding method varies in heat input, weld quality, metallurgical influence, and compatibility with different materials.

TIG welding (Gas Tungsten Arc Welding, GTAW) uses a non-consumable tungsten electrode and inert shielding gas (argon/helium) to produce high-purity welds with precise heat control. This makes it ideal for thin sections and reactive alloys (aluminum, titanium) but requires skilled operation and is comparatively slow (Kou, 2003; Sathiya *et al*., 2019).

The localized heating-cooling cycle in TIG welding generates significant residual stresses due to constrained thermal expansion/contraction. These stresses induce distortion, cracking, and accelerated fatigue failure, compromising structural integrity (Lindgren, 2001; Deng, 2018).

There are different types of expert methods for simulation some of which are Computation Fluid dynamics (CFD) for weld pool dynamics. This simulates fluid flow, heat transfer, and mass transport in the molten weld pool, Microstructure Evolution Modeling is used for predicting phase transformations, Machine Learning (ML) Augmented Simulations, and SIMUFACT software.

Computational mechanics, particularly the SIMUFACT software, enables high-fidelity simulation of welding thermo mechanics. By modeling temperature-dependent material behavior and transient thermal cycles, SIMUFACT predicts residual stress distributions, identifies critical stress zones, and optimizes welding parameters (Goldak and Akhlaghi, 2005; Muránsky *et al.,* 2019).

1.2 STATEMENT OF THE PROBLEM

Residual stresses in TIG weldments frequently exceed design limits, leading to premature failures. Analytical models fail to capture 3D stress complexity, resulting in unresolved industrial challenges like, Distortion and Warping (Non-uniform thermal gradients cause buckling and misalignment, affecting dimensional accuracy (Kou, 2003; Adak *et al*., 2020)), Cracking (Solidification shrinkage (hot cracks) and hydrogen embrittlement (cold cracks) initiate at stress-concentrated zones (Elmesalamy *et al*., 2018)), Fatigue Life Reduction (Residual stresses lower fatigue strength by 30–50%, especially at weld toes and heat-affected zones (HAZ) (Lindgren, 2001; Farajian-Sohi *et al*., 2021)).

Applying SIMUFACT to simulate the actual maximum stress in TIG weldment will therefore aid in mitigating against structural failure resulting from stress concentration in welded joint.

1.3 AIM AND OBJECTIVES

The aim of this project is to develop a robust predictive model, leveraging the SIMUFACT software, to understand and control the actual maximum stress induced in Tungsten Inert

Gas (TIG) weldments

To achieve this aim, the following specific objectives will be pursued:

I. Conduct a review of recent relevant existing literature on SIMUFACT simulation of the mechanical properties in TIG welded joints

II. Identify necessary TIG welding process (input) parameters and their range of values from previous studies.

III. To generate a robust experimental matrix using a suitable design expert component.

IV. Conduct TIG welding experiments on mild steel coupons and record the actual maximum stress values in the experimental samples.

V. Simulate the experimental result using SIMUFACT.

VI. carry out comparative analysis on the experimental and SIMUFACT result.

VII. ascertain their degree of correlation

1.4 SCOPE OF THE STUDY

The scope of this study is limited to the simulation of the actual maximum stress in a TIG weldment using the SIMUFACT software by studying the effect of current, voltage and gas flow rate in TIG weldment stress concentration.

1.5 SIGNIFICANCE OF THE STUDY

This study will focus on the SIMUFACT simulation of the actual maximum stress in TIG weldments. The study will consider the effects of various parameters, including welding speed, heat input, and material properties, on the stress distribution in the weldment. TIG welding underpins safety-critical components in nuclear, aerospace, and chemical industries. Residual stresses remain a leading cause of in-service failures, yet experimental measurement (hole-drilling, neutron diffraction) is costly and limited in resolution (Deng, 2018; Kumar, 2020). Computational SIMUFACT simulation offers a robust, economical alternative to Predict stress hotspots inaccessible to sensors, optimize parameters to mitigate distortion/cracking, and Extend service life of welded structures (Pandey *et al*., 2021).

This study bridges the gap between simulation fidelity and industrial reliability, advancing design protocols for high-performance weldments.

CHAPTER TWO

LITERATURE REVIEW

2.1 Welding Process: Concept of Welding

Welding is a fabrication process that joins materials, typically metals or thermoplastics, through high heat, pressure, or both, causing coalescence. The process may involve the use of filler materials to facilitate the joint and sometimes shielding gases to protect the weld pool from atmospheric contamination. The fundamental principle behind welding is the application of heat or pressure to the base metals, leading to their fusion at the interface (Kou, 2003). Welding plays an indispensable role in industries like automotive, aerospace, construction, shipbuilding, and energy due to its efficiency in forming permanent joints with high mechanical strength.

The effectiveness of a welding process depends on factors such as material compatibility, heat input, joint design, and environmental conditions. The evolution of welding technologies has transitioned from forge welding in ancient times to advanced processes like laser and electron beam welding today (Kalpakjian and Schmid, 2014).

2.2 Types of Welding

Welding techniques are broadly classified based on the energy source and method of heat application. The main types include:

2.2.1 Arc Welding: Utilizes an electric arc between an electrode and the base material. Examples include Shielded Metal Arc Welding (SMAW), Gas Metal Arc Welding (GMAW), and TIG welding (Miller, 2010). Arc welding is a fusion welding process used to join metals. An electric arc from an AC or DC power supply creates an intense heat of around 6500°F which melts the metal at the join between two work pieces.

The arc can be either manually or mechanically guided along the line of the join, while the electrode either simply carries the current or conducts the current and melts into the weld pool at the same time to supply filler metal to the join. Because the metals react chemically to oxygen and nitrogen in the air when heated to high temperatures by the arc, a protective shielding gas or slag is used to minimize the contact of the molten metal with the air. Once cooled, the molten metals solidify to form a metallurgical bond.

This process can be categorized into two different types; consumable and non-consumable electrode methods.

2.2.1.1 Consumable Electrode Methods

2.2.1.1.1 Metal Inert Gas Welding (MIG) and Metal Active Gas Welding (MAG)

Also known as Gas Metal Arc Welding (GMAW), uses a shielding gas to protect the base metals from contamination.

2.2.1.1.2 **Shielded Metal Arc Welding (SMAW)**

Also known as manual metal arc welding (MMA or MMAW), flux shielded arc welding or stick welding is a process where the arc is struck between the metal rod (electrode flux coated) and the work piece, both the rod and work piece surface melt to form a weld pool. Simultaneous melting of the flux coating on the rod will form gas, and slag, which protects the weld pool from the surrounding atmosphere. This is a versatile process ideal for joining ferrous and non-ferrous materials with a range of material thicknesses in all positions.

2.2.1.1.3 Flux Cored Arc Welding (FCAW)

Created as an alternative to SMAW, FCAW uses a continuously fed consumable flux cored electrode and a constant voltage power supply, which provides a constant arc length. This process either uses a shielding gas or just the gas created by the flux to provide protection from contamination.

2.2.1.1.4 Submerged Arc Welding (SAW)

A frequently-used process with a continuously-fed consumable electrode and a blanket of fusible flux which becomes conductive when molten, providing a current path between the part and the electrode. The flux also helps prevent spatter and sparks while suppressing fumes and ultraviolet radiation.

2.2.1.1.5 Electro-Slag Welding (ESW)

A vertical process used to weld thick plates (above 25mm) in a single pass. ESW relies on an electric arc to start before a flux addition extinguishes the arc. The flux melts as the wire consumable is fed into the molten pool, which creates a molten slag on top of the pool. Heat for melting the wire and plate edges is generated through the molten slag's resistance to the passage of the electric current. Two water-cooled copper shoes follow the process progression and prevent any molten slag from running off.

2.2.1.1.6 Arc Stud Welding (SW)

Similar to flash welding, SW joins a nut or fastener, usually with a flange with nubs that melt to create the join, to another metal piece.

2.2.1.2 Non-consumable Electrode Methodsu

2.2.1.2.1 Tungsten Inert Gas Welding (TIG)

Also known as Gas Tungsten Arc Welding (GTAW), uses a non-consumable tungsten electrode to create the arc and an inert shielding gas to protect the weld and molten pool against atmospheric contamination.

2.2.1.2.2 Plasma Arc Welding (PAW)

Similar to TIG, PAW uses an electric arc between a non-consumable electrode and an anode, which are placed within the body of the torch. The electric arc is used to ionize the gas in the torch and create the plasma, which is then pushed through a fine bore hole in the anode to reach the base plate. In this way, the plasma is separated from the shielding gas.

2.2.2 Gas Welding: Gas welding, also known as oxy-fuel welding or oxy-acetylene welding, is a fusion welding process that uses the combustion of oxygen and a fuel gas (commonly acetylene) to generate a high-temperature flame for melting and joining metals. The process involves directing a flame from a hand-held torch onto the metal surfaces to be joined, which are heated to a molten state and allowed to fuse upon cooling (Kalpakjian and Schmid, 2014). A filler metal may also be added to enhance joint strength, depending onthe welding application.

Gas welding comprises several types based on the fuel gas used in combination with oxygen or air. Each type generates different flame temperatures, combustion properties, and suitability for particular applications. Below are the major types of gas welding:

2.2.2.1 Oxy-Acetylene Welding (OAW)

This is the most widely used type of gas welding. It utilizes a mixture of oxygen and acetylene to produce a flame temperature of approximately 3,200°C, which is sufficient to weld most ferrous and non-ferrous metals. The flame type can be adjusted (neutral, carburizing, oxidizing) to suit different metals.

Applications: Mild steel, aluminum, brass, and copper.

Advantages: High flame temperature, precise flame control, and versatility.

Disadvantages: Acetylene is expensive and unstable at high pressure.

2.2.2.2 Oxy-Hydrogen Welding (OHW)

This process uses hydrogen as the fuel gas instead of acetylene. The flame temperature is lower, approximately 2,000°C, making it more suitable for light work, such as welding thin sheets, lead, and aluminum. Its applications are Jewelry, dental tools, thin sheet welding.

Advantages: Clean flame, no carbon contamination, hydrogen is readily available.

Disadvantages: Lower flame temperature limits its use for heavy-duty welding.

2.2.3 Resistance Welding: Resistance welding is a pressure welding process in which the heat required to join metals is generated by electrical resistance to current flow at the interface of the workpieces. It involves clamping two or more metal parts together and passing a controlled electrical current through them for a specific time. The heat generated by the resistance causes localized melting or plastic deformation at the contact surface, resulting in a welded joint once pressure is applied and the area cools.

This process does not require filler material, flux, or shielding gas, making it clean and suitable for high-volume production (Kalpakjian and Schmid, 2014).

There are different types of resistance welding and some of which are

2.2.3.1 Spot Welding: This is the most common form of resistance welding. The process involves placing overlapping metal sheets between two copper electrodes and applying current to create a weld spot. they are used in Automobile body panels, metal furniture, domestic appliances. It has High speed, good reproducibility, low operator skill required.

2.2.3.2 Seam Welding: Similar to spot welding, but the electrodes are rotating wheels that create a continuous weld seam. They are used in Fuel tanks, steel drums, and radiators. It has Leak-proof welds, automated process suitable for high-volume production.

2.2.3.3 Projection Welding: Utilizes localized projections or embossments on one of the workpieces to concentrate current and pressure. Multiple welds can be made in a single operation. They are used in Nut and bolt welding, electrical terminals. It is Efficient for mass production and complex assemblies.

2.2.3.4 Flash Butt Welding: The Ends of two metal parts are brought together and heated using an arc caused by electrical resistance, then forged under pressure. They are used for Joining of rails, rods, and tubes. It has High strength joint, suitable for heavy sections.

2.2.4 Solid-State Welding Solid-state welding is a category of welding processes in which coalescence (joining) of materials occurs without the materials reaching their melting point. Unlike fusion welding processes, solid-state welding does not involve molten phases. Instead, it relies on the application of pressure, sometimes with heat below the melting temperature, and sometimes with mechanical deformation, to produce a metallurgical bond between the joining surfaces.

This technique is particularly useful for joining dissimilar metals and materials that are difficult to weld using conventional fusion processes, and it minimizes issues like residual stress, distortion, and phase transformation associated with melting and solidification. (Cary and Helzer, 2005).

Some common types of solid-state welding use are

2.2.4.1 Friction Welding (FRW): In this welding Heat is generated through mechanical friction between the workpieces, Pressure is applied to forge the parts together. This welding is Suitable for cylindrical components like shafts and rods.

2.2.4.2 Ultrasonic Welding (USW): This welding Uses high-frequency ultrasonic vibrations under moderate pressure. It is Commonly used for plastics and thin metal sheets and Frequently used in electronics, automotive, and medical device manufacturing.

2.2.4.3 Diffusion Welding: In this welding Bonding occurs through atomic diffusion at the interface it Requires high pressure and elevated temperature over a long time. It is Ideal for aerospace applications and joining dissimilar metals.

2.2.4.4 Explosion Welding (EXW): This welding is carried out by High-velocity impact caused by a controlled detonation which is Capable of joining large surface areas and dissimilar metals. It is Common in cladding operations (bonding stainless steel to carbon steel).

2.2.4.5 Forge Welding (FOW): It is the Traditional blacksmith technique, It Involves heating metals to a plastic state and hammering them together. It is Still used in artistic and heritage metalworking.

2.2.4.6 Cold Welding: This type of welding Takes place at room temperature with sufficient pressure. It is Effective for very ductile and clean metals like aluminum and copper.

2.3 Categories of Welding

Welding processes are categorized based on their operational principles:

2.3.1 Fusion Welding

Fusion welding is a category of welding processes where the base metals are melted at the joint interface to form a coalesced bond. This type of welding may or may not involve the use of filler materials, and often requires external heat sources such as electric arcs, flames, lasers, or electron beams. In contrast to solid-state welding, fusion welding involves actual melting and solidification, resulting in the formation of a heat-affected zone (HAZ).

Fusion welding is the most widely used welding process in various industries due to its versatility, ability to join complex geometries, and adaptability to both manual and automated systems.

There are different types of fusion welding some of which are

2.3.1.1 Arc Welding: This Utilizes an electric arc between an electrode and the base metal to generate heat. It Includes subtypes like:

a. Shielded Metal Arc Welding (SMAW) (a.k.a. stick welding)
b. Gas Metal Arc Welding (GMAW/MIG)
c. Gas Tungsten Arc Welding (GTAW/TIG)
d. Flux-Cored Arc Welding (FCAW)

2.3.1.2 Gas Welding: It Uses a flame produced by burning a fuel gas (like acetylene) with oxygen (Oxy-fuel welding). Oxy-acetylene is the most common and suitable for thin materials and repairs.

2.3.1.3 Laser Beam Welding (LBW): It uses High-energy laser beam to melt and join materials. It Offers precise, high-speed, and deep penetration welding. It is Common in electronics, automotive, and medical device industries.

2.3.1.4 Electron Beam Welding (EBW): It Uses a high-velocity beam of electrons in a vacuum to create heat that Allows very deep and narrow welds with minimal distortion. It is Applied in aerospace and nuclear industries.

2.3.1.5 Plasma Arc Welding (PAW): It is Similar to TIG but uses a constricted plasma arc for higher energy concentration. It is Suitable for precision welding of thin materials.

2.3.1.6 Solid-State Welding Solid-state welding is a category of welding processes in which coalescence (joining) of materials occurs without the materials reaching their melting point. Unlike fusion welding processes, solid-state welding does not involve molten phases. Instead, it relies on the application of pressure, sometimes with heat below the melting temperature, and sometimes with mechanical deformation, to produce a metallurgical bond between the joining surfaces.

This technique is particularly useful for joining dissimilar metals and materials that are difficult to weld using conventional fusion processes, and it minimizes issues like residual stress, distortion, and phase transformation associated with melting and solidification. (Cary and Helzer, 2005).

Some common types of solid-state welding use are

a. Friction Welding (FRW): In this welding Heat is generated through mechanical friction between the workpieces, Pressure is applied to forge the parts together. This welding is Suitable for cylindrical components like shafts and rods.

b. Ultrasonic Welding (USW): This welding Uses high-frequency ultrasonic vibrations under moderate pressure. It is Commonly used for plastics and thin metal sheets and Frequently used in electronics, automotive, and medical device manufacturing.
c. Diffusion Welding: In this welding Bonding occurs through atomic diffusion at the interface it Requires high pressure and elevated temperature over a long time. It is Ideal for aerospace applications and joining dissimilar metals.
d. Explosion Welding (EXW): This welding is carried out by High-velocity impact caused by a controlled detonation which is Capable of joining large surface areas and dissimilar metals. It is Common in cladding operations (bonding stainless steel to carbon steel).
e. Forge Welding (FOW): It is the Traditional blacksmith technique, It Involves heating metals to a plastic state and hammering them together. It is Still used in artistic and heritage metalworking.
f. Cold Welding: This type of welding Takes place at room temperature with sufficient pressure. It is Effective for very ductile and clean metals like aluminum and copper.

2.3.1.6 High-Energy Beam Welding: High-Energy Beam Welding (HEBW) refers to a group of advanced welding processes that utilize highly concentrated energy beams either in the form of electrons or lasers to join materials. These processes produce deep-penetration, narrow welds with minimal distortion, making them suitable for applications requiring high precision, such as in aerospace, electronics, and nuclear industries.

The two main types of HEBW are:

a. Electron Beam Welding (EBW)
b. Laser Beam Welding (LBW)

Both are fusion welding processes and are typically performed in a vacuum or with protective shielding to prevent oxidation and ensure weld integrity.

2.3.1.7.1 Electron Beam Welding (EBW)

EBW uses a focused beam of high-velocity electrons, which strike the workpiece and convert kinetic energy into heat. This heat melts the metal at the joint, forming a weld.

Features:

a. Conducted in a vacuum chamber to prevent electron scattering.
b. Achieves deep weld penetration with narrow heat-affected zones.
c. Welds are clean, precise, and high-strength.

Advantages:

a. Ideal for dissimilar metal joints.
b. Produces minimal distortion.
c. Capable of welding thick and reactive materials (titanium, molybdenum).

Limitations:

a. Expensive equipment and maintenance.
b. Limited to vacuum-compatible components.
c. Not suitable for high-production environments without automation.

2.3.1.7.2 Laser Beam Welding (LBW)

LBW uses a concentrated laser beam usually from a CO_2, or fiber laser as a heat source to melt and join materials. It can be carried out in air or inert gas shielding, depending on material sensitivity.

Features:

a. Can be performed atmospherically or in a controlled environment.
b. Compatible with automation and robotics.
c. Offers high-speed welding with minimal post-processing.

Advantages:

a. Suitable for thin and thick sections.
b. Provides excellent control over weld depth and width.
c. High repeatability and low thermal distortion.

Limitations:

a. Initial setup cost is high.
b. Requires precise joint fit-up and alignment.
c. Reflective materials (like aluminum) may pose challenges. *(American Welding Society (AWS). (2020))*

2.3.1.8 Thermochemical Welding: Thermochemical welding is a group of welding processes in which chemical reactions usually exothermic (heat-releasing) reactions are used to generate the heat necessary to melt and join metals. These processes do not require an external power source like electricity or gas. Instead, they rely on the chemical energy stored in a mixture of reactive compounds, typically metal oxides and reducing agents, to produce extremely high temperatures capable of melting the base metals and creating a strong metallurgical bond.

The most widely known thermochemical welding process is thermite welding (also called exothermic welding).

2.3.1.8.1 Thermite Welding (Exothermic Welding)

Thermite welding involves a chemical reaction between metal oxides (commonly iron(III) oxide) and a metallic reducing agent (usually aluminum powder). This reaction, known as the Goldschmidt reaction, generates molten metal and intense heat (up to 2500 °C), which is used to fuse metal parts usually steel.

Reaction Equation:

$Fe_2O_3 + 2Al \rightarrow 2Fe(molten) + Al_2O_3 + heat$

Features:

a. No external power source needed.

b. Produces molten steel that fills a preformed mold around the joint.

c. Commonly used for field welding of railway tracks, pipelines, and rebar.

Advantages of Thermochemical Welding:

a. No electricity or gas supply required, ideal for remote locations.

b. Produces high-strength, homogeneous joints.

c. Simple setup and operation.

d. Can weld large cross-sections.

e. Ideal for outdoor and emergency repairs.

Disadvantages:

a. Single-use process and each weld requires a fresh thermite charge and mold.

b. Long cooling time; not suited for mass production.

c. Difficult to control weld parameters (heat input, cooling rate).

d. Generates intense heat and sparks and requires careful safety measures.

e. Not suitable for thin materials or non-ferrous metals. Goldschmidt, H. (1904).

2.4 TIG Welding

Tungsten Inert Gas (TIG) welding, also known as Gas Tungsten Arc Welding (GTAW), is a precision welding process that uses a non-consumable tungsten electrode to produce the weld. The weld area is shielded from atmospheric contamination by an inert gas, typically argon or helium, and a filler metal may or may not be used depending on the application.

TIG welding is widely used in industries where high weld quality, precision, and clean appearance are essential. This includes sectors such as aerospace, automotive, pressure vessels, nuclear, and chemical processing. The process is highly suitable for welding thin materials, especially non-ferrous metals like aluminum, magnesium, and titanium, as well as stainless steel.

2.4.1 Advantages of TIG Welding

TIG welding offers several advantages over other welding methods:

a. High Weld Quality: Produces clean, high-strength, and aesthetically pleasing welds with minimal spatter and distortion (Kou, 2003).
b. No Slag Formation: Since TIG does not use flux, no slag is formed, reducing post-weld cleaning.
c. Precise Control: Excellent control over heat input and weld pool, allowing for thin material welding (Messler, 2004).
d. No Spatter: TIG welding is spatter-free, which makes it ideal for surfaces requiring high finish.
e. Versatile: Suitable for a wide range of materials, including aluminum, copper alloys, stainless steel, titanium, and magnesium (AWS, 2020).
f. Autogenous Welding: Can be performed without filler metal, particularly for autogenous welds in thin sections. (Miller, 2010).

2.4.2 Disadvantages of TIG Welding

Despite its benefits, TIG welding has some limitations:

a. Low Deposition Rate: Compared to MIG or SMAW, TIG welding is slower, especially for thicker materials.

b. High Skill Requirement: Requires a skilled operator due to manual control of the electrode, torch, and filler rod simultaneously.
c. Equipment Cost: TIG welding equipment is more expensive and complex due to the use of high-frequency start systems and gas flow control (Kalpakjian and Schmid, 2014).
d. Limited Outdoor Use: Inert shielding gases are easily displaced by wind, making TIG less suitable for outdoor or draughty environments.
e. Preparation Time: Requires clean surfaces and proper joint preparation to avoid contamination and porosity.

2.4.3 TIG Welding Process Parameters

Key parameters influencing weld quality include:

a. Welding Current:
    I. DCEN (Direct Current Electrode Negative) for welding steels and stainless steels.
    II. AC (Alternating Current) for non-ferrous metals like aluminum and magnesium.
    III. Typical current range: 5–300 A.
b. Voltage:
    I. Depends on arc length and shielding gas.
    II. Generally ranges between 10–20 V.
c. Shielding Gas:
    I. Argon: Most common, provides stable arc and smooth bead.
    II. Helium: Increases heat input and penetration.

III. Mixtures: Argon-helium mixtures used for deeper penetration and faster welding.

d. Tungsten Electrode:

Types: Pure tungsten, thoriated, ceriated, lanthanated.

Diameter: 1.0 mm to 4.0 mm depending on current and material.

e. Torch Angle: Typically held at 10°–15° from vertical (push angle).

f. Travel Speed: Affects bead width and penetration; must be optimized for consistent weld quality.

g. Filler Metal:

I. Optional; should be compatible with base metal.

II. Introduced manually into the weld pool.

h. Pre- and Post-Flow Gas Timing: Ensures protection of the weld pool and tungsten electrode before and after arc initiation. (Zhang *et al*., 2022).

(Withers and Bhadeshia, 2001).

2.5 Induced Stress and Its Effect in Weldment

During welding, a localized heat source melts the base metal and often a filler metal, creating a weld pool that subsequently cools and solidifies. This non-uniform thermal cycle results in expansion and contraction, which introduce residual stresses commonly known as induced stresses within the weld and adjacent base metal. These stresses can significantly affect the mechanical performance, dimensional stability, and integrity of welded structures.

Induced stresses arise primarily due to the thermal gradients and restraint conditions during the welding process and can persist in the material as residual stresses even after the weld

cools down (Kou, 2003). The magnitude and distribution of these stresses depend on various factors such as welding parameters, joint configuration, material properties, and heat input.

2.5.1 Categories of Induced Stress

Induced stresses in weldments can be broadly classified into three categories:

2.5.1.1 Thermal Stress

Thermal stress is caused by the uneven temperature distribution during welding. As different zones of the metal expand and contract at different rates, internal stresses are generated. These stresses may lead to warping, distortion, or even cracking if not controlled properly (Masubuchi, 1980).

2.5.1.2 Residual Stress

Residual stress is the locked-in stress that remains in the material after welding and cooling, in the absence of external forces. It can be:

a. Tensile Residual Stress – typically found in the weld metal and heat-affected zone (HAZ); it can promote crack initiation.
b. Compressive Residual Stress – may occur in areas surrounding tensile zones; it can be beneficial in resisting crack propagation.

2.5.1.3 Mechanical Stress

Mechanical stress results from external constraints or loading during or after welding. Fixtures, clamps, or misaligned components can contribute to these stresses.

2.5.2 Effects of Induced Stress on Welded Structures

Induced stress has significant implications for the structural performance and longevity of welded components:

2.5.2.1 Distortion and Warping

Due to the non-uniform thermal expansion and contraction, welded structures often exhibit bending, twisting, or buckling, which compromises dimensional accuracy (Liu *et al*., 2022).

2.5.2.2 Reduced Fatigue Life

Tensile residual stresses in the weld zone can act as stress concentrators, leading to premature fatigue failure, especially under cyclic loading.

2.5.2.3 Cracking and Fracture

High levels of residual tensile stress, especially in brittle materials or under restrained conditions, can cause hot cracking (solidification cracking), cold cracking, or delayed cracking.

2.5.2.4 Stress Corrosion Cracking (SCC)

In corrosive environments, the presence of tensile residual stress can accelerate corrosion-assisted crack growth, especially in materials like stainless steel or aluminum alloys (Sridhar *et al*., 2004).

2.5.2.5 **Dimensional Instability**

Welded components with unbalanced residual stresses may undergo distortion over time, especially after machining or heat treatment.

2.5.3 Mitigation of Induced Stress

To minimize or control induced stress in welded structures, several techniques are employed:

2.5.3.1 Preheating

Preheating the base material before welding reduces the temperature gradient, helping to lower thermal and residual stresses.

2.5.3.2 Post-Weld Heat Treatment (PWHT)

This involves heating the welded structure to a specific temperature and holding it for a period to relieve residual stresses and improve toughness.

2.5.3.3 Controlled Welding Parameters

a. Using low heat input
b. Balanced weld sequences
c. Backstep welding
d. Intermittent welding can reduce the stress accumulation in multi-pass welds.

2.5.3.4 Mechanical Stress Relief Methods

a. Peening: Deforming the surface plastically to introduce compressive stresses.
b. Vibration stress relief: Uses mechanical vibrations to redistribute stresses.

2.5.3.5 SIMUFACT Simulation

Numerical techniques such as SIMUFACT simulation can predict stress distribution in welds and help in optimizing process parameters to reduce stress concentrations (Zhang et al., 2021).

2.6 Actual Maximum Stress

In the context of welded joints, actual maximum stress refers to the highest localized stress occurring in a structure due to welding-induced factors, such as thermal expansion, phase transformation, geometry discontinuities, and material heterogeneity. Unlike nominal stress, which is calculated based on average load and geometry, actual maximum stress

accounts for stress concentrations, residual stresses, and localized effects that arise particularly in critical zones such as the weld toe, root, and heat-affected zone (HAZ).

Understanding the actual maximum stress is essential for ensuring the structural integrity, fatigue life, and safety of welded components, especially those subjected to cyclic loading or harsh environmental conditions (Kou, 2003; Zhang *et al.*, 2021).

2.6.1 Causes of Actual Maximum Stress in Welded Structures

Actual maximum stress arises due to a combination of the following factors:

2.6.1.1 Welding Residual Stress: Caused by non-uniform thermal cycles during welding, resulting in high tensile stresses.

2.6.1.2 Stress Concentration at Weld Geometry: Weld toes, undercuts, and discontinuities often create regions of sharp gradients in stress.

2.6.1.3 Material Inhomogeneity: The weld metal, base metal, and HAZ often possess differing mechanical properties, contributing to stress mismatches.

2.6.1.4 External Loading Conditions: In-service loads combined with residual stresses may amplify local stress states.

2.6.1.5 Thermal Expansion and Shrinkage: The differential expansion and contraction of welded materials leads to stress accumulation, particularly in constrained joints (Masubuchi, 1980).

2.6.2 Methods for Measuring Actual Maximum Stress

Several methods exist for quantifying actual maximum stress in welded components, broadly classified into experimental, analytical, and numerical approaches.

2.6.2.1 **Experimental Methods**

2.6.2.1.1 Strain Gauges

a. Small devices affixed to the surface to measure strain, which can be converted to stress using Hooke's Law.
b. Limited to surface measurements and requires high-resolution placement.

2.6.2.1.2 X-Ray Diffraction (XRD)

c. Measures changes in atomic spacing due to residual stress.
d. Non-destructive and highly accurate for surface-level stress analysis.

2.6.2.1.3 Hole Drilling Method

Involves drilling a small hole at the point of interest and measuring the relieved strain. It is Semi-destructive but widely used for residual stress determination.

2.6.2.1.4 Digital Image Correlation (DIC)

A full-field, non-contact optical method for measuring deformation and strain distribution.

2.6.2.1.5 Photoelasticity

Experimental technique using birefringent materials to visualize stress patterns. Primarily qualitative, but useful for stress concentration studies.

2.6.2.2 Analytical Methods

Analytical approaches often use closed-form equations and fracture mechanics principles to estimate the actual maximum stress. For example:

a. Stress concentration factors (SCFs) from standard geometries (fillet welds) help calculate amplified stress based on notch effects.
b. Nominal stress method combined with SCFs:

$\sigma max = Kt \cdot \sigma nominal$

Where Kt is the theoretical stress concentration factor.

2.6.2.3 Application of SIMUFACT in simulating welding process.

SIMUFACT Welding is a specialized software used to simulate and analyze various welding processes, including Tungsten Inert Gas (TIG), MIG, and resistance welding. It helps engineers predict how heat and stress develop in a welded structure during and after welding. The software uses temperature-dependent material properties and process parameters such as current, voltage, welding speed, and gas flow rate to model the real welding environment. It provides visual and numerical results showing temperature distribution, residual stress, distortion, and deformation in the weldment (Hexagon, 2023; Kou, 2021).

By applying SIMUFACT, researchers can optimize welding parameters, reduce defects, and minimize the number of experimental trials required. This makes it a powerful and cost-effective tool for predicting actual maximum stress and improving the quality of welded joints (Li and Zhang, 2020).

2.7 Stress Simulation Techniques

Stress simulation techniques are vital analytical tools used to predict, analyze, and visualize stress distribution within materials and structures under different loading and thermal conditions. In the context of welded joints, stress simulation helps identify critical zones, such as the weld bead, toe, and heat-affected zone (HAZ), where failure is most likely to initiate due to residual or operational stresses.

By simulating stress behavior, engineers can optimize weld design, select appropriate materials, and establish safe loading limits without the cost and time associated with physical testing. This is especially important in high-risk industries such as aerospace, marine, and nuclear power, where structural failure could be catastrophic (Kou, 2003).

Stress simulations are broadly categorized into analytical, numerical, and hybrid methods, depending on the complexity of the structure and desired accuracy.

2.8 SIMUFACT SIMULATION

SIMUFACT Welding is a process-oriented simulation software developed by Hexagon Manufacturing Intelligence for analyzing joining processes. It predicts heat transfer, distortion, and residual stress in welded structures using material-specific thermal and mechanical data (Hexagon, 2023; Kou, 2021).

2.8.1 Welding Parameters and Boundary Conditions

The welding parameters applied in the simulation are consistent with experimental settings: current (170–190 A), voltage (22–25 V), and gas flow rate (14–17 L/min). The plates were assumed to be at room temperature (25°C) before welding. Mechanical constraints were applied to simulate clamping, while convection and radiation losses were considered at the free surfaces (Kou, 2021).

2.9 Safety Procedures in TIG Welding

Safety procedures in welding are essential to ensure the health and protection of personnel, prevent accidents, and maintain equipment integrity. Tungsten Inert Gas (TIG) welding, although relatively clean and precise, still involves high temperatures, ultraviolet radiation, electrical hazards, and potential exposure to toxic fumes. As such, stringent safety protocols must be followed throughout the welding process, especially in research or industrial environments where high-fidelity simulations or physical experiments are conducted.

2.9.1 Personal Protective Equipment (PPE)

Proper PPE is critical to protect welders from burns, electric shocks, radiation, and inhalation hazards. Key equipment includes:

a. Welding Helmet with Auto-darkening Filter (ADF): Protects the eyes and face from UV/IR radiation and molten splatter.
b. Fire-resistant Clothing: Made from flame-retardant materials (e.g., treated cotton or leather) to protect skin from burns.
c. Gloves: Heat-resistant, insulated welding gloves to guard against heat and electric shock.
d. Safety Boots: Steel-toed, electrical-insulated boots with non-slip soles.
e. Respiratory Protection: Fume extraction masks or powered air-purifying respirators (PAPR) when welding alloys that emit hazardous fumes (e.g., stainless steel or aluminum).

According to OSHA Standard 1910.252, appropriate PPE is mandatory for all welding operations.

2.9.2 Electrical Safety

TIG welding uses high-frequency AC or DC power sources, which can pose serious electrical hazards if not handled properly.

a. Ensure Proper Grounding: Welding equipment and workpieces must be properly grounded to prevent electric shock.
b. Inspect Cables and Leads: Cables should be intact, insulated, and free from wear or cracking.
c. Dry Environment: Welding should never be done in damp or wet conditions; hands and clothing should also be dry.
d. Switch Off When Idle: The power supply should be turned off when not in use to prevent unintentional arcing.

Electric shock from welding circuits can cause severe injury or death. Voltages as low as 50V can be dangerous under wet conditions (Jeffus, 2020).

2.9.3 Fire and Explosion Prevention

The high temperature of the arc (~6000°C) poses a serious fire hazard.

a. Remove Flammable Materials: Ensure the work area is free of paper, oil, fuel, or plastic containers.
b. Use Fire Blankets: Cover nearby equipment and surfaces to contain sparks and hot metal.
c. Keep Fire Extinguishers Nearby: A Class C fire extinguisher should be accessible at all times.
d. Ensure Proper Ventilation: Prevent accumulation of flammable gases in confined spaces.

NFPA 51B outlines fire watch procedures during hot work operations.

2.9.4 Ventilation and Fume Extraction

Although TIG welding produces fewer fumes than other methods, welding certain metals (e.g., stainless steel, nickel alloys) can still generate toxic oxides and ozone.

a. Local Exhaust Ventilation (LEV): Should be used to capture fumes at the source.
b. General Ventilation: Maintain adequate airflow to reduce fume concentration.
c. Fume Monitoring: Use sensors for hazardous substances like hexavalent chromium.

Inhalation of welding fumes is associated with long-term health risks, including metal fume fever and lung cancer (IARC, 2017).

2.9.5 UV Radiation Protection

TIG welding emits intense ultraviolet (UV) and infrared (IR) radiation that can cause skin burns and “arc eye” (photokeratitis).

a. Use Welding Curtains: To protect others nearby from exposure.

b. Wear UV-blocking PPE: Helmets, gloves, and clothing rated for UV protection.

c. Limit Exposure: Avoid looking directly at the arc even briefly.

2.9.6 Safe Handling of Tungsten Electrodes and Shielding Gas

a. Tungsten Handling: Use gloves when handling tungsten electrodes, especially thoriated types that may emit alpha radiation.

b. Shielding Gas Cylinders (Argon):

- Store upright and secure to prevent tipping.
- Never expose to heat or sparks.
- Open valves slowly to prevent pressure surges.

Compressed gas cylinders must comply with safety standards (ASME BPVC, OSHA 29 CFR 1910.101).

2.9.7 Ergonomics and Workspace Safety

a. Proper Positioning: Workpieces should be clamped at a comfortable height to reduce strain.

b. Lighting: Adequate lighting is essential to prevent mistakes and reduce eye strain.

c. Trip Hazards: Remove cables or tools from walkways to prevent falls.

2.9.8 Emergency Procedures

a. First Aid Kit: Must be stocked and accessible.

b. Emergency Contact: All personnel should know whom to call and where emergency exits are.

c. Burn Treatment: Cool burns with water and seek medical assistance immediately.

CHAPTER THREE

METHODOLOGY

In the previous chapter we made a perspective sketch of the various relevant research works surrounding the present research study. In this chapter we shall explain the research strategy to be employed to obtain and analyze data for the study. The methodological steps are as follows;

i. Identification of input parameters range

ii. Samples and sampling technique

iii. Experimental data collection

iv. Experimental data analysis

3.1 Identification of Input Parameters Range.

The key parameters to be considered in this work are welding current (A), welding voltage (V), Gas Flow Rate (L/Min). The range of the process parameters to be used were gotten from relevant recent literature is tabulated below.

Table 3.1: Process parameters and their levels

PARAMETERS	UNITS	SYMBOL	MINIMUM VALUE	MAXIMUM VALUE
Welding Current	Amps	I	160.00	190.00
Welding Voltage	Volts	V	22.00	25.00
Gas Flow Rate	L/Min	GFR	14.00	17.00

Erhunmwunse B.O and Ozigagun A. (2021).

The following materials and equipment would be used to effectively and successfully carry out this research study: mild steel plates, power hacksaw, a TIG welding machine, argon gas and a Universal Stress Testing machine.

3.2 Samples and sampling technique

The weld samples will be made from mild steel plates and cut to size using hack saw, edges grinded, surface polished with emery paper and the joint welded. A tungsten inert gas welding equipment will be used to carry out the welding process on the mild steel plates. The TIG welding process will use a shielding gas to protect the weld specimen from atmospheric interaction, 100% pure Argon gas will be used for this research study. The TIG welding machine alongside the argon gas is as shown in fig. 3.1.

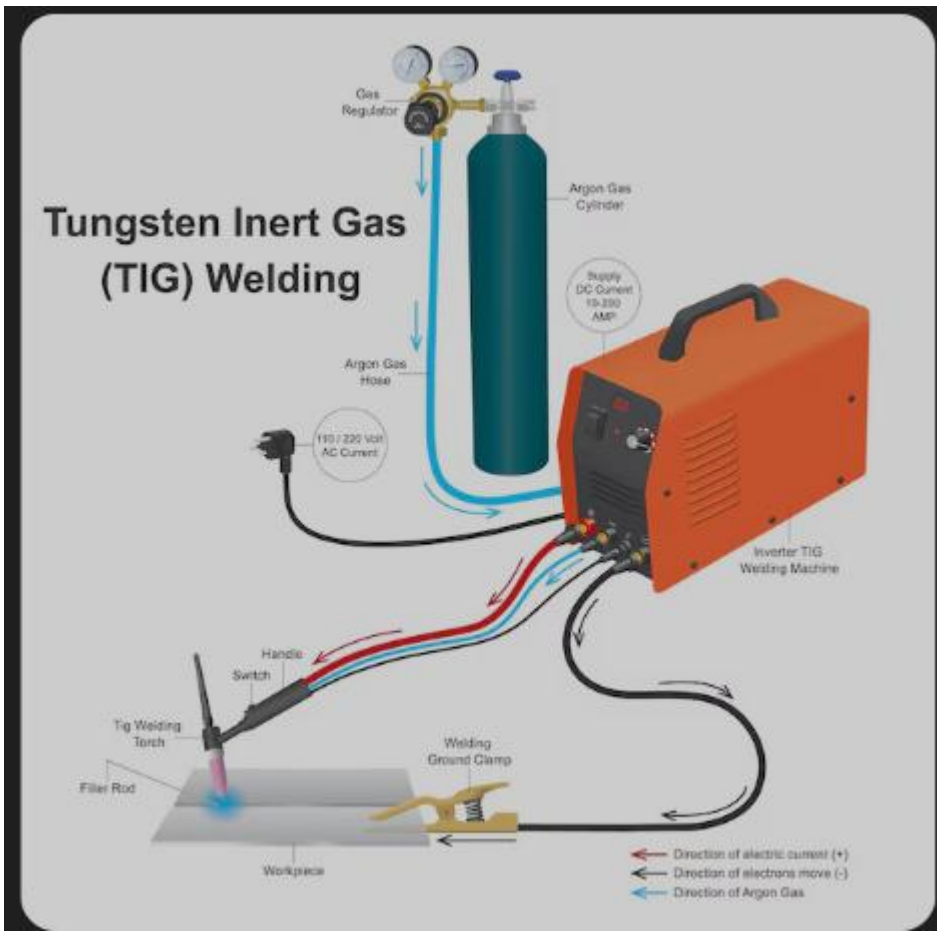

Fig 3.1: TIG equipment with argon gas cylinder

Fig. 3.2: Argon gas cylinder

Universal Stress Testing Machine

A Universal Stress Testing Machine (commonly known as a Universal Testing Machine, or UTM) is a multi-purpose material testing instrument used to evaluate the mechanical properties of materials under various types of loading conditions, such as 48 tension, compression, bending, and shear. It is termed “universal” because it can perform a wide range of standardized mechanical tests on diverse materials including metals, plastics, ceramics, polymers, and composites (Budynas and Nisbett, 2015).

Fig.3.3 Universal stress testing machine

3.3 Experimental Data Collection

The input parameters (Current, Voltage and Gas flow rate) will be used as factors for the design matrix. The central composite design (CCD) interphase of VERSION 13.05 Design Expert will be used to developed a statistical design of experiment. The CCD matrix utilizing the three input parameter generated an experimental design matrix having six (6) center points (n_o), six (6) axial points (2n) and eight (8) factorial points (2^n) which when imputed into Equation 3.1 resulted in twenty (20) experimental runs. The CCD matrix is presented in Table 3.2. The total number of experimental runs as generated by the CCD is given as:

$$N = 2^n + n_o + 2n \tag{3.1}$$

where;

N: is the number of experimental runs based on CCD, 2^n: is the number of factorial points, n_o: is the number of center points, 2n: is the number of axial points and n: is the number of variables. Table 3.2 shows the experimental matrix generated by the CCD.

Table 3.2 Central Composite Design (CCD) Experimental Matrix Factors

Run	Factor 1	Factor 2	Factor 3
	A: Current (Amp)	B: Voltage (Volt)	C: Gas Flow Rate (lit/min)
1	170	22	14
2	170	23	15
3	190	24	16
4	170	25	17
5	180	22	15
6	170	23	16
7	180	24	17
8	160	25	14
9	180	22	16
10	160	23	17
11	160	24	14
12	160	25	15
13	180	22	17
14	170	23	14
15	170	24	15
16	170	25	16
17	170	25	17
18	170	24	14
19	160	23	15
20	170	22	16

3.4 Experimental Data Analysis

In this study, the SIMUFACT simulation software is used as a numerical tool to analyze stress distribution in TIG-welded joints. The simulation provides virtual experimental data that replicates real-world welding conditions, helping to determine stress concentration factors (SCF) and identify critical stress zones.

The analysis begins with creating a CAD model of the weldment, followed by meshing, applying boundary conditions, and assigning material properties. Loads simulating thermal and mechanical effects from welding are applied. The simulation then calculates stress and strain distributions across the model.

From the results, the maximum stress near the weld toe and the nominal stress in the base material are used to compute the SCF using:

$$K_t = \sigma_{max}$$

This method allows for detailed, cost-effective analysis of weld performance, aiding in failure prediction and design optimization.

CHAPTER FOUR

RESULTS AND DISCUSSION

This chapter presents the results obtained from both the experimental tests and the SIMUFACT simulations conducted using SIMUFACT Welding 2024. The study aims to predict and validate the actual maximum stress developed in Tungsten Inert Gas (TIG) welded joints under varying process parameters. The results are organized into three parts:

(i) presentation of actual experimental data,

(ii) simulation of the welding process using SIMUFACT

(iii) Presentation of SIMUFACT result

(iv) Comparison between the actual experimental result and the SIMUFACT result

4.1 Presentation of The Experimental Results

The experimental phase involved TIG welding of low carbon steel plates (S235) under systematically varied process parameters—welding current, voltage, and shielding gas flow rate. The welded specimens were mechanically tested to determine the maximum stress sustained by each weldment.

Table 4.1: Experimental Results for TIG Welded Samples

Run	Current (A)	Voltage (V)	Gas Flow (L/min)	Experimental Maximum Stress (MPa)
1	170	22	14	355.04
2	170	23	15	354.97
3	190	24	16	311.28
4	170	25	17	319.7
5	180	22	15	354.44
6	170	23	16	353.97
7	180	24	17	316.02
8	160	25	14	353.26
9	180	22	16	352.85
10	160	23	17	357.3
11	160	24	14	349.07
12	160	25	15	355.52
13	180	22	17	355.85
14	170	23	14	355.75
15	170	24	15	344.11
16	170	25	16	317.48
17	170	25	17	316.46
18	170	24	14	345.6
19	160	23	15	357.14
20	170	22	16	355.73

Observations shows that the ranges of welding current is from 160A-190A, voltage is from 22V-25V and gas flow rate is from 14L/min – 17L/min. The experimental results show that the maximum stress values ranged between 311 MPa and 357 MPa, with the highest value (357.30 MPa) recorded at a relatively low current (160 A) and voltage (23 V). This suggests that higher heat input reduces the cooling rate, thereby lowering residual stress, whereas lower currents produce sharper thermal gradients and higher stress accumulation.

4.2 Simulation of The Welding Process Using SIMUFACT

The experimental welding process parameters were replicated in SIMUFACT Welding 2024, using a thermomechanical arc welding process model with double-ellipsoidal heat source distribution. The simulated model included two S235-SPM-sw mild steel plates joined in a butt joint configuration, with clamping at both ends and a total welding time of 22 seconds.

The material properties, boundary conditions, and solver settings were as follows:

i. Process type: Arc welding (manual)
ii. Ambient temperature: 20 °C
iii. Welding velocity: 5 mm/s
iv. Heat input (net): 6732 J/cm
v. Efficiency: 0.9
vi. Solver: MUMPS parallel direct solver (4 processors)
vii. Total time: 22 s (0–22 s)
viii. Elements: 3,280 solid elements and 5,262 surface elements

The simulated low carbon steel S256 plates as developed by SIMUFACT is as shown in Figure 4.1

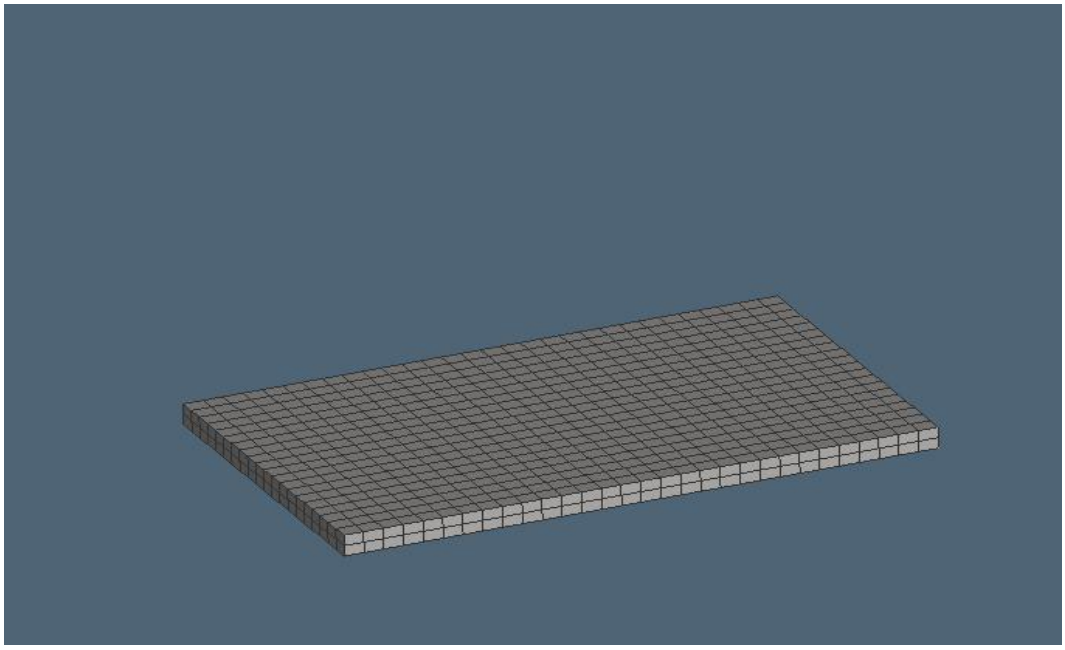

Fig.4.1 TWO S235-SPM-SW MILD STEEL PLATES

Time intervals of trajectories

The time trajectory ranges from 00s to 22s from start time to end time

Process report

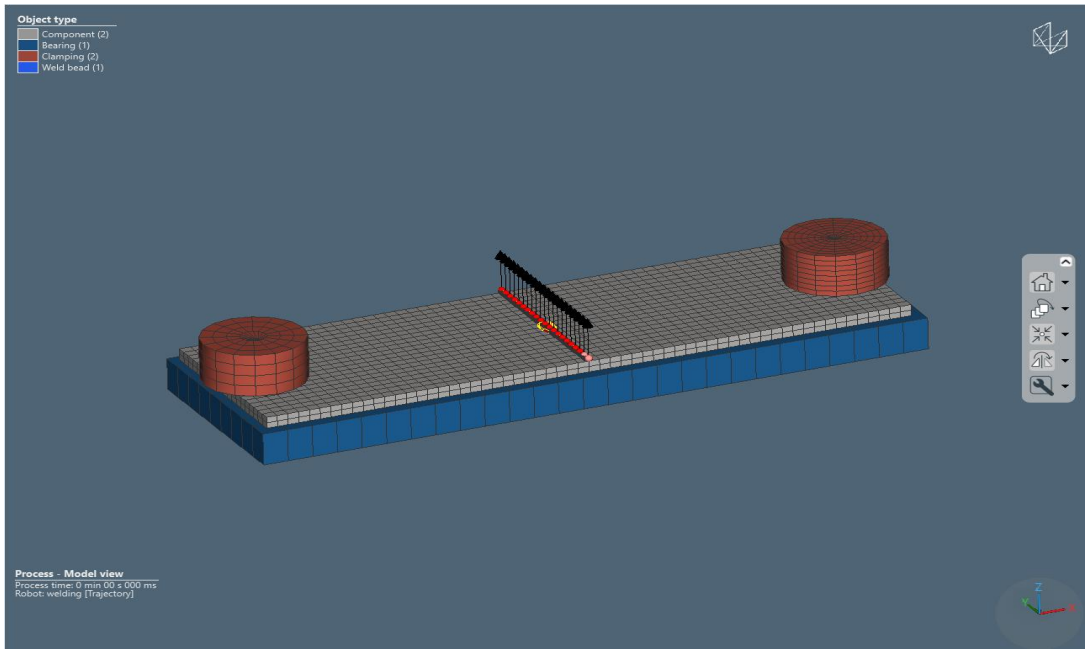

Fig. 4.3 COMPONENT, BEARING, CLAMPING AND WELD BEAD

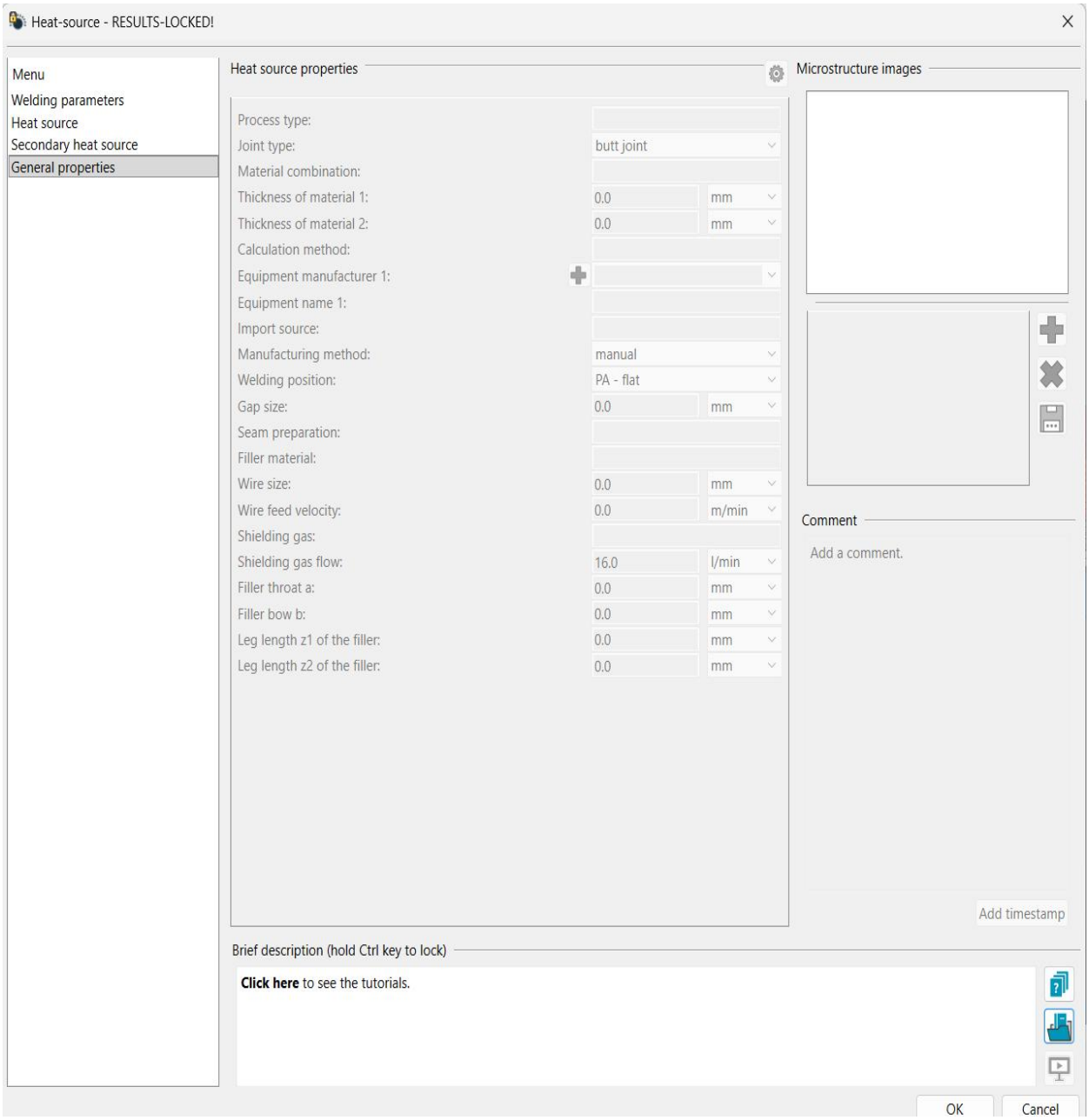

Fig.4.4 input parameters of the shielding gas flow rate and weld type

Process parameters

a) Process type: Arc welding

b) Shrinkage active: no

c) Single-shot solution: no

d) Solution: Thermomechanical

e) Symmetry plane: not available

f) Ambient temperature: 20.0 °C

Process Parameters Explanation

In carrying out the simulation analysis, several process parameters were defined to ensure accurate and efficient computation of the forming operation. The solver type selected was MUMPS (Multifrontal Massively Parallel Sparse) Parallel Direct, a highly efficient numerical solver capable of handling large and complex finite element models. It employs a parallel direct matrix solution method that allows the program to perform simultaneous calculations across multiple processors, thereby improving computational speed and staz\ability. To further enhance performance, multiprocessing with four processors was activated, allowing the simulation to utilize four CPU cores for faster data processing and reduced solution time.

The phase transformation option was not used in this analysis. This means that the simulation focused solely on the mechanical deformation behavior of the material without accounting for any temperature-induced changes in the material's microstructure. This approach is suitable when the forming process occurs under conditions where phase changes are negligible or not of interest. Additionally, high-end contact separation with prevention of chattering was employed. This parameter improves the accuracy of surface contact interactions between the die and the workpiece, ensuring that contact and separation occur smoothly. The prevention of chattering helps to avoid numerical instabilities and oscillations that can occur when surfaces repeatedly make and lose contact, leading to more realistic simulation results.

Finally, the domain decomposition was set to one domain, meaning that the model was solved as a single continuous computational region. This simplifies the numerical process and ensures consistent convergence of results, particularly when dealing with moderately sized models that do not require extensive parallel subdivision.

Analysis Time and Model Refinement Parameters Explanation

The analysis time in the simulation was defined with a start time of 0.0 seconds and an end time of 22.0 seconds, indicating that the entire forming or welding process was numerically observed over a 22-second duration. This range represents the total time interval in which deformation, heat transfer, and other process responses were computed. The time step calculation was set to fixed (automatic), meaning that the software automatically controlled the size of each time increment during computation. This ensures numerical stability and accuracy by adjusting the time step according to the process dynamics, especially during complex interactions such as contact or heat input phases.

For the result time steps, a cooling time of 5.0 seconds was applied. This setting enabled the simulation to capture the cooling behavior of the workpiece after the primary forming or heating operation. The inclusion of cooling time allows for a more realistic thermal response, as temperature gradients and residual stresses often develop during this stage.

The refinement parameters were set with a refinement level of 0, meaning that no additional mesh refinement was applied to the model. In SIMUFACT analysis, refinement refers to increasing the mesh density in regions of high stress or thermal gradients to obtain more accurate results. Since the refinement level was zero, the standard mesh resolution was considered sufficient for the simulation's objectives. Additionally, the heat source area scaling factor was set to 1.2, which slightly

expanded the effective area influenced by the applied heat source. This adjustment helps to better represent the actual heat distribution within the material during the simulated process.

The global unrefinement settings were configured with the type set to “none” and level set to 0, indicating that no automatic coarsening of the mesh occurred during the simulation. Unrefinement is typically used to reduce computational load by coarsening the mesh in regions where deformation or temperature change is minimal. However, by turning it off, the analysis maintained a consistent mesh density throughout the process, ensuring uniform accuracy. The “prevent unrefinement in contact area” option was also set to off, meaning that the mesh in contact regions was not restricted from adjustment, though no unrefinement occurred in this case.

Table 4.2

Loadcase times

Number	Start time [s]	Stop time [s]	Initial time step	Minimum time step	Maximum time step	Steps	Loadcase	Loadcase name
1	0.0	22.0	0.624856	1e-06	0.624856	36	Welding	welding_1

ComponentsIn the simulation setup, two primary components were defined: *plate-mm* and *plate-mm-2*. Both components were assigned the same base material, **S235-SPM-sw**, which is a structural steel commonly used in welding and mechanical simulations due to its predictable mechanical behavior and weldability. The initial temperature for each component was set at **20.0°C**, representing ambient room temperature conditions prior to the application of thermal and mechanical loads. The geometric definitions of the components were identified as *plate-mm* and *plate-mm-2*, respectively, corresponding to the modeled weld plates in the simulation environment. Neither of the components was used as filler material, as indicated by the inactive filler setting. Furthermore, there were no result value transfers available at this stage, implying that no preliminary computational data were carried over from prior analyses. This configuration establishes the foundational parameters for the TIG weldment simulation, ensuring that both plates begin under identical initial conditions for accurate stress and thermal response comparison during the welding process. The SIMUFACT welding process was set in the following conditions.

i. In the welding simulation, several boundary and process conditions were defined to ensure realistic modeling of the TIG welding operation. The analysis was conducted over a total duration of **22.0 seconds**, beginning at **0.0 seconds** and ending at **22.0 seconds**, representing the complete thermal and mechanical cycle of the welding process. A **bearing geometry** was included in the model to provide necessary support and constrain specific degrees of freedom during the simulation. However, the process did not incorporate any fixed geometries or fixed nodes, indicating that the plates were free to expand or contract under thermal loads within the constraints provided by the bearings and clamps.

ii. Two **clamping conditions**—identified as *Clamping* and *Clamping-2*—were

applied at the start of the analysis to stabilize the plates throughout the welding process. Each clamp was assigned a **spring stiffness of 1000.0 N/m** and a **holding force of 0.05 kN**, ensuring controlled restraint without over-constraining the model. These parameters simulate the practical conditions used to secure workpieces during TIG welding operations, minimizing distortion while allowing limited thermal expansion.

iii. The simulation did not employ any **local joints** or **virtual pins**, confirming that no additional localized constraints or rotational joints were introduced in the setup. For the **robotic welding operation**, a **standard robot** model was utilized with an ambient **temperature of 20.0°C**, corresponding to room temperature conditions. The robot executed a single **weld bead** along a **trajectory length of 110.0 mm**, with the same total working time of **22.0 seconds**. The welding trajectory and associated **heat source parameters** were predefined and controlled to ensure accurate simulation of heat input and weld pool development during the process.

iv. This configuration collectively represents a realistic setup for thermal–mechanical simulation in TIG welding using SIMUFACT Welding software, ensuring accurate prediction of induced stress, heat distribution, and deformation behavior across the weldment.

Table 4.3Time summary

Order	Trajectory	Length	Start welding	End welding	Welding time	End time	Welding parameter	Welding filler
1	Trajectory	110.0 mm	0.0 s	22.0 s	22.0 s	22.0 s	Heat-source	Trajectory-weldbead

Geometrical and Material Properties Configuration for simulation

The simulation model comprised multiple geometrical components, including *plate-mm*, *plate-mm-2*, *bearing*, *clamping*, *clamping-2*, and *trajectory-weldbead*. Each of these geometries was defined to replicate the real TIG welding setup as accurately as possible. Both *plate-mm* and *plate-mm-2* were modeled in millimeters, with each surface mesh consisting of 1402 nodes and 1400 elements, while the corresponding volume model contained 1953 nodes and 1200 elements. These two plates represent the base materials joined during welding. The bearing geometry, modeled in meters, provided essential mechanical support, consisting of 560 nodes and 558 elements on its surface, with no volume model defined. Similarly, the clamping geometries (*clamping* and *clamping-2*) were used to restrain the plates during welding, having 368 nodes and 380 elements, and 176 nodes and 188 elements, respectively, in their surface models. The trajectory-weld bead geometry represented the path of the weld bead, modeled in meters, consisting of 1338 nodes and 1336 elements in its surface model, and 1665 nodes with 880 elements in its volume mesh. This geometric definition ensured adequate mesh refinement in critical regions such as the weld zone and heat-affected areas to capture temperature gradients and stress distributions effectively.

The base material, *S235-SPM-sw*, was generated from multiphase model data with an initial phase composition of 93% ferrite and 7% pearlite, neglecting transformation effects. The alloy composition was obtained from JMatPro and comprised approximately 0.15% C, 0.4% Cu, 98.29% Fe, 1.1% Mn, 0.01% N, 0.02% P, and 0.027% S, with an austenitization temperature of 1300°C and a cooling rate of 171.01°C/s. The grain size corresponded to ASTM 7.51, and flow curves were calculated with an initial microstructure size of 30 microns. The Poisson's ratio for this material was set to 0.3, while its electrical properties were referenced from Wink and Krätschmer (2012).

The filler material, *SG1-JMP-MPM-sw*, was similarly defined using JMatPro version 6.2. Its alloy composition included approximately 0.1% C, 0.65% Si, 1.1% Mn, 0.15% Mo, 0.15% Ni, 0.15% Ti, and 97.68% Fe, with a corresponding ASTM grain size of 11.71 and an austenitization temperature of 1300°C. The cooling rate was 196.92°C/s, and a Poisson's ratio of 0.3 was adopted. These material definitions ensured accurate modeling of thermal conductivity, yield behavior, and phase response during the heating and cooling cycles of TIG welding.

The welding trajectory was globally oriented and consisted of 21 data points, all of which were active during the simulation, representing a continuous weld path along the plate joint. The heat source was defined as a conventional TIG welding model with a butt joint configuration and a flat (PA) welding position, consistent with typical TIG welding setups. Although filler parameters such as wire size and feed velocity were not explicitly modeled, shielding gas flow was defined as 0.000266667 m^3/s, providing inert gas protection during the simulated process. The welding current and voltage were set to 170 A and 22 V, respectively, producing a gross energy input of 7480 J/cm and a net energy input of 6732 J/cm with an assumed efficiency of 0.9. The welding speed was maintained at 5.0 mm/s, under a transient specification mode using indirect power control.

The heat source geometry parameters included a front length of 2.89 mm, a rear length of 11.57 mm, a width of 3.99 mm, and a penetration depth of 8.30 mm, representing the molten pool dimensions during welding. These parameters were scaled using a heat front factor of 0.4 to simulate the Gaussian heat distribution typical of TIG arcs. Collectively, these inputs provided a comprehensive thermal–mechanical environment for the simulation, enabling accurate computation of temperature gradients, thermal stress development, and residual stress distribution within the TIG-welded S235 steel plates. The individual simulation by SIMUFACT for the 20 runs are depicted as follows:

Run 1:

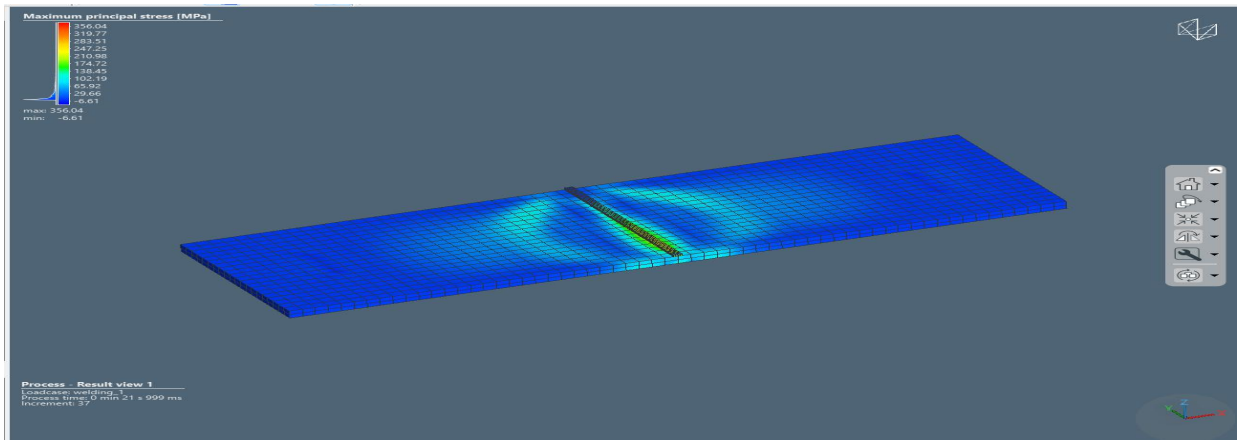

Fig.4.5 SIMUFACT simulation: RUN 1

The image shows the simulated maximum principal stress distribution in a TIG-welded joint, with peak stress (356.04 MPa) concentrated along the weld zone. The stress gradually decreases toward the base plates, indicating localized thermal and residual stress effects.

Run 2:

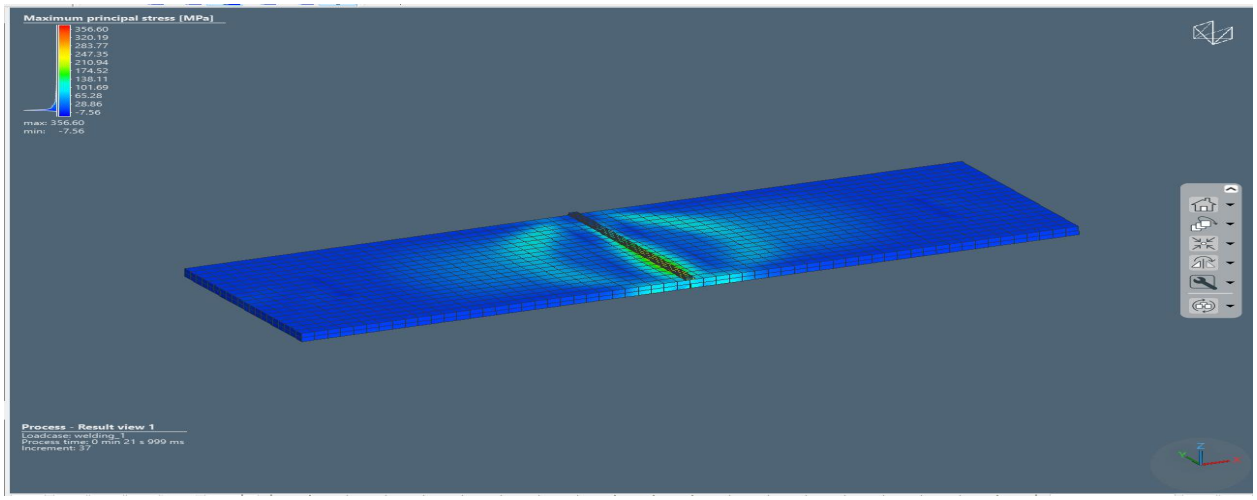

Fig.4.6 SIMUFACT simulation: RUN 2

The image shows the simulated maximum principal stress distribution in a TIG-welded joint, with peak stress (356.60 MPa) concentrated along the weld zone. The stress gradually decreases toward the base plates, indicating localized thermal and residual stress effects.

3rd Run

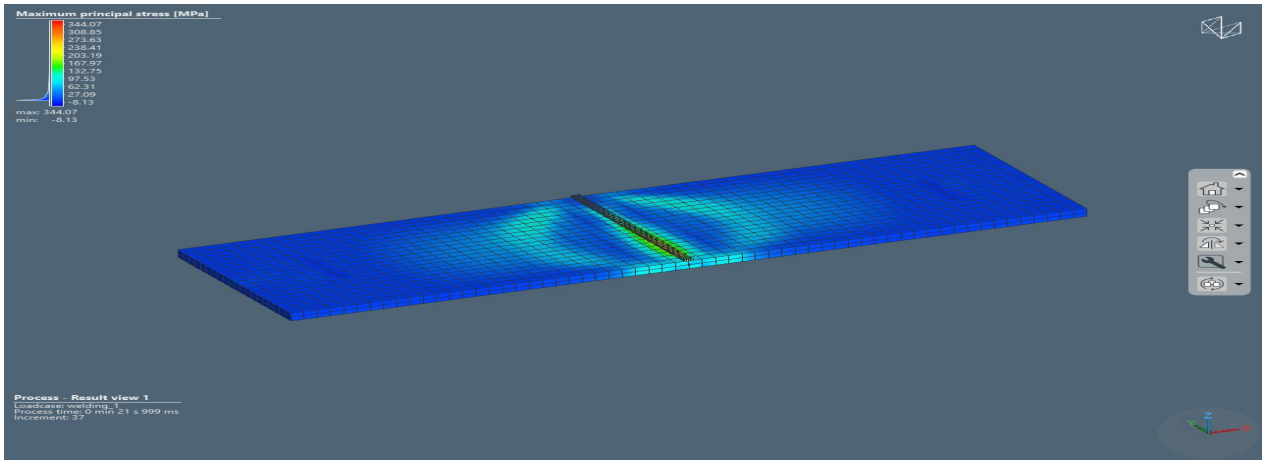

Fig.4.7 SIMUFACT simulation: RUN 3

The image shows the simulated maximum principal stress distribution in a TIG-welded joint, with peak stress (344.07 MPa) concentrated along the weld zone. The stress gradually decreases toward the base plates, indicating localized thermal and residual stress effects.

4th RUN

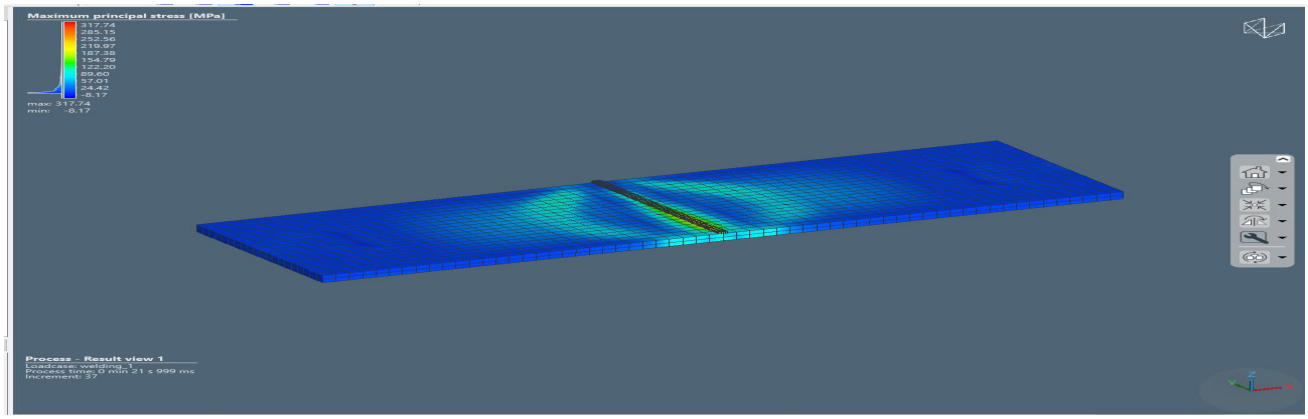

Fig.4.8 SIMUFACT simulation: RUN 4

The image shows the simulated maximum principal stress distribution in a TIG-welded joint, with peak stress (317.74 MPa) concentrated along the weld zone. The stress gradually decreases toward the base plates, indicating localized thermal and residual stress effects.

5TH RUN

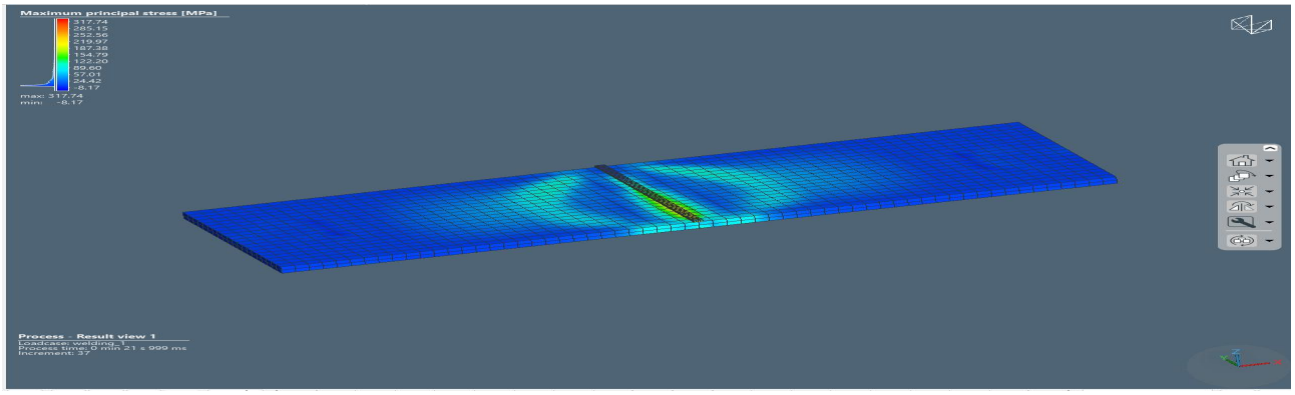

Fig.4.9 SIMUFACT simulation: RUN 5

The image shows the simulated maximum principal stress distribution in a TIG-welded joint, with peak stress (317.74 MPa) concentrated along the weld zone. The stress gradually decreases toward the base plates, indicating localized thermal and residual stress effects.

6TH RUN

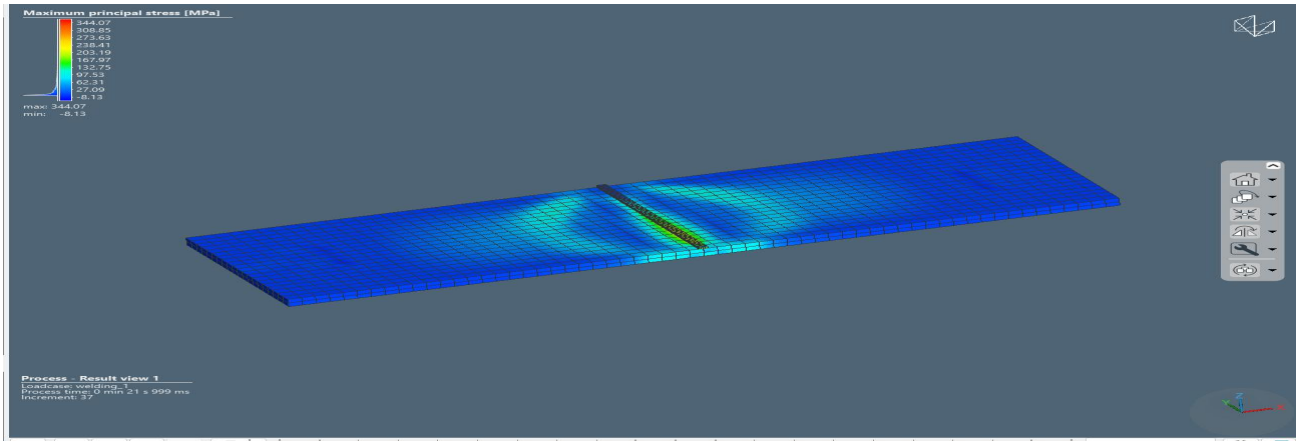

Fig.4.10 SIMUFACT simulation: RUN 6

The image shows the simulated maximum principal stress distribution in a TIG-welded joint, with peak stress (344.07 MPa) concentrated along the weld zone. The stress gradually decreases toward the base plates, indicating localized thermal and residual stress effects.

7TH RUN

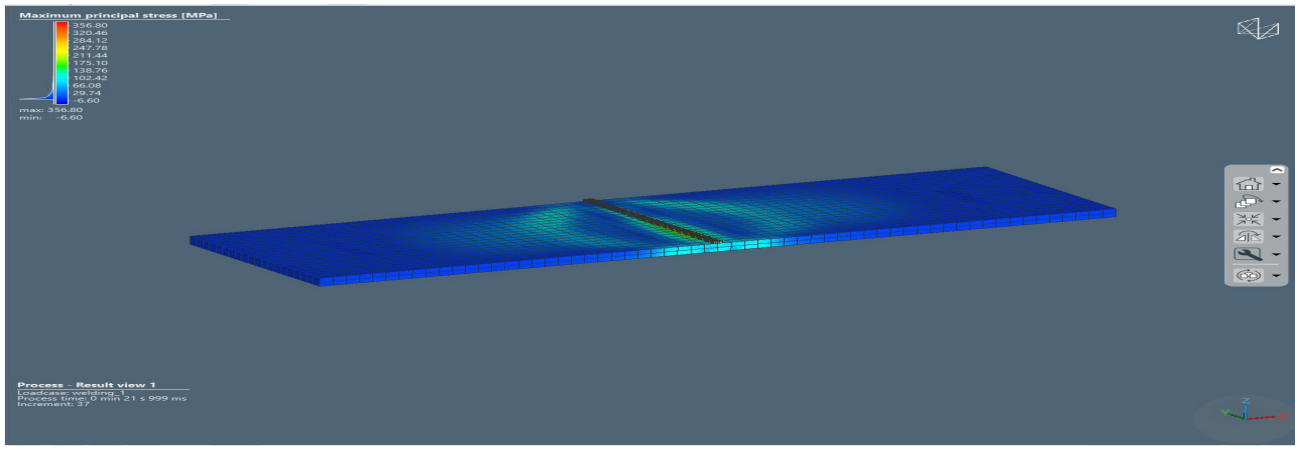

Fig.4.11 SIMUFACT simulation: RUN 7

The image shows the simulated maximum principal stress distribution in a TIG-welded joint, with peak stress (356.80 MPa) concentrated along the weld zone. The stress gradually decreases toward the base plates, indicating localized thermal and residual stress effects.

8TH RUN

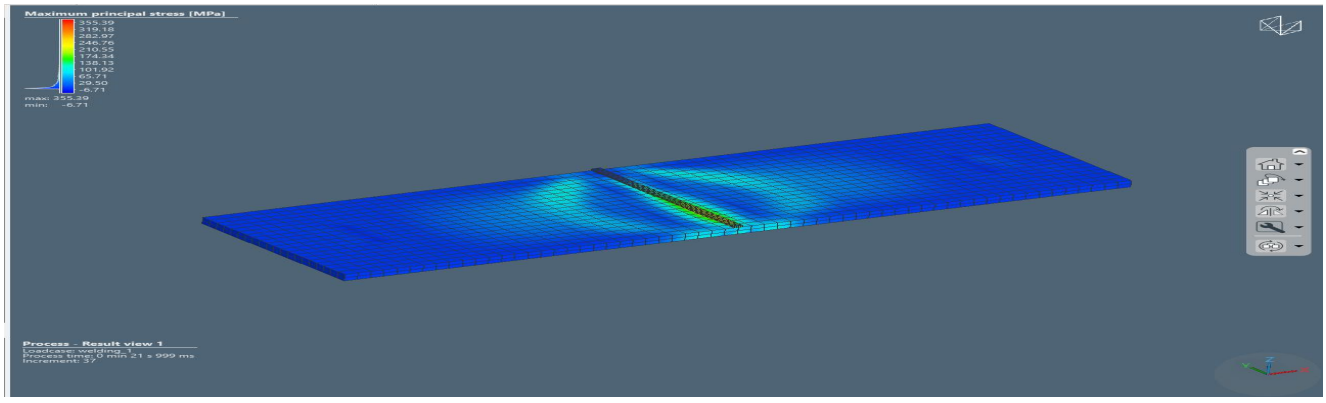

Fig.4.12 SIMUFACT simulation: RUN 8

The image shows the simulated maximum principal stress distribution in a TIG-welded joint, with peak stress (355.39 MPa) concentrated along the weld zone. The stress gradually decreases toward the base plates, indicating localized thermal and residual stress effects.

9TH RUN

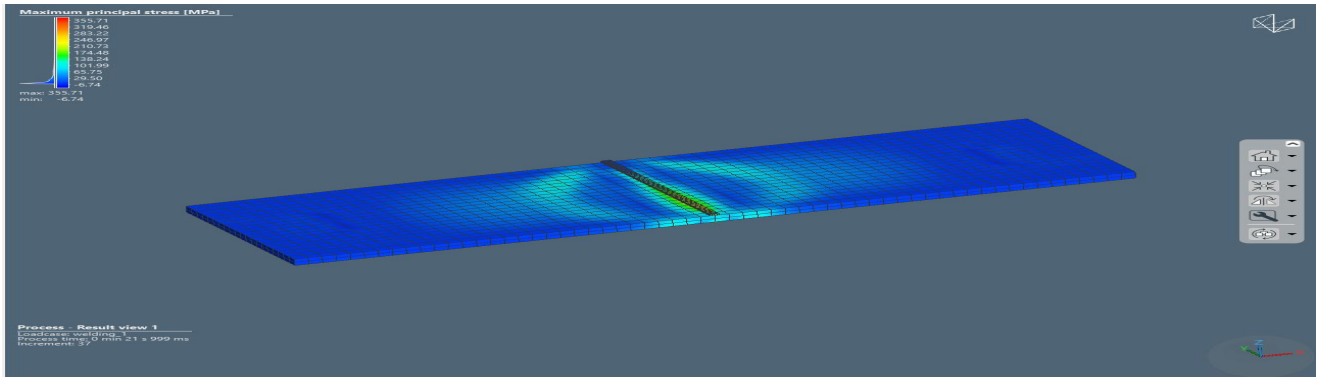

Fig.4.13 SIMUFACT simulation: RUN 9

The image shows the simulated maximum principal stress distribution in a TIG-welded joint, with peak stress (355.71 MPa) concentrated along the weld zone. The stress gradually decreases toward the base plates, indicating localized thermal and residual stress effects.

10TH RUN

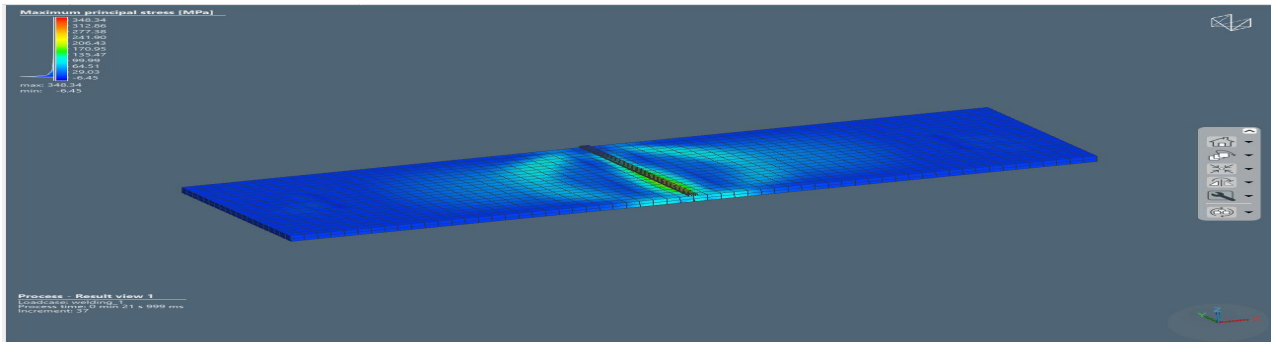

Fig.4.14 SIMUFACT simulation: RUN 10

The image shows the simulated maximum principal stress distribution in a TIG-welded joint, with peak stress (348.34 MPa) concentrated along the weld zone. The stress gradually decreases toward the base plates, indicating localized thermal and residual stress effects.

11TH RUN

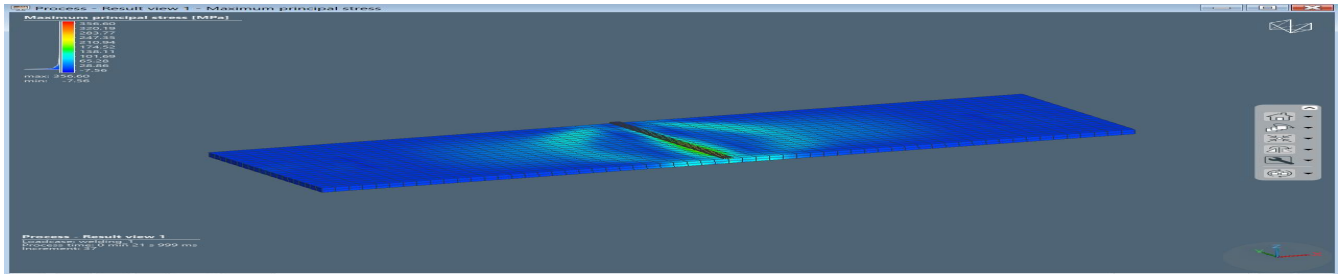

Fig.4.15 SIMUFACT simulation: RUN 11

The image shows the simulated maximum principal stress distribution in a TIG-welded joint, with peak stress (356.60 MPa) concentrated along the weld zone. The stress gradually decreases toward the base plates, indicating localized thermal and residual stress effects.

12TH RUN

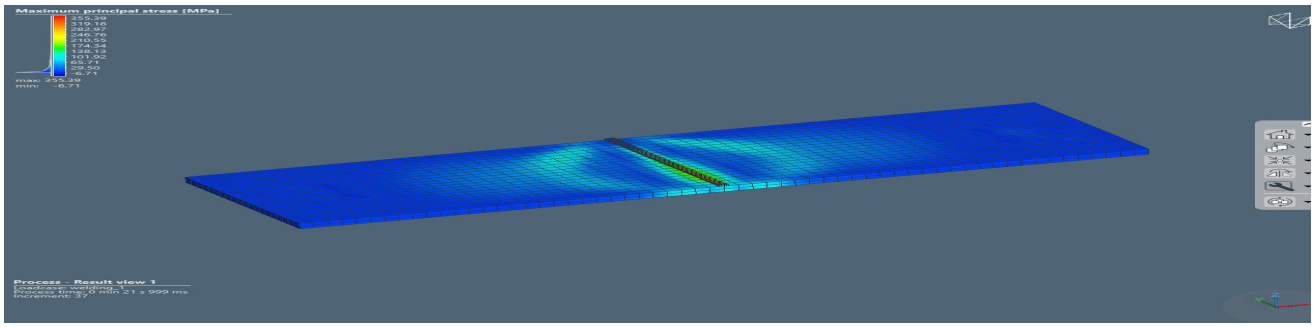

Fig.4.16 SIMUFACT simulation: RUN 12

The image shows the simulated maximum principal stress distribution in a TIG-welded joint, with peak stress (355.39 MPa) concentrated along the weld zone. The stress gradually decreases toward the base plates, indicating localized thermal and residual stress effects.

13TH RUN

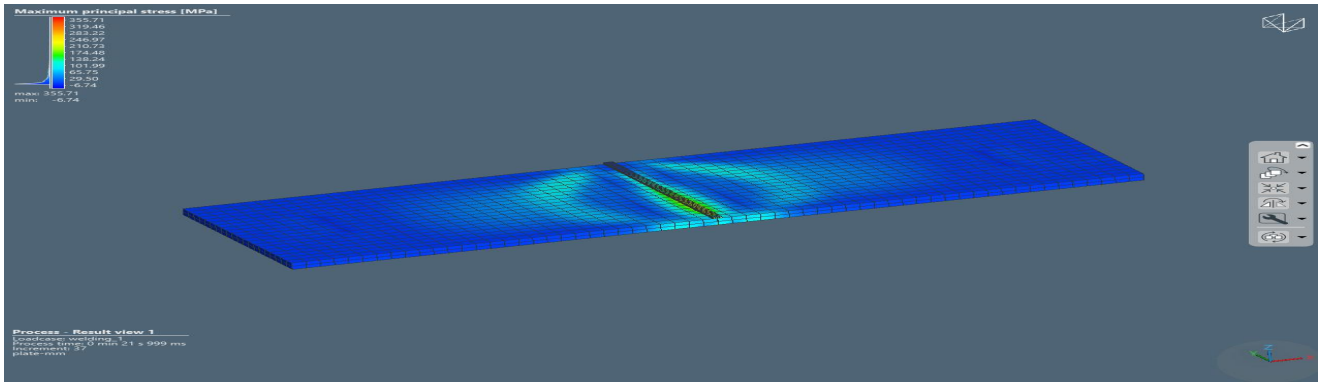

Fig.4.17 SIMUFACT simulation: RUN 13

The image shows the simulated maximum principal stress distribution in a TIG-welded joint, with peak stress (355.71 MPa) concentrated along the weld zone. The stress gradually decreases toward the base plates, indicating localized thermal and residual stress effects.

14TH RUN

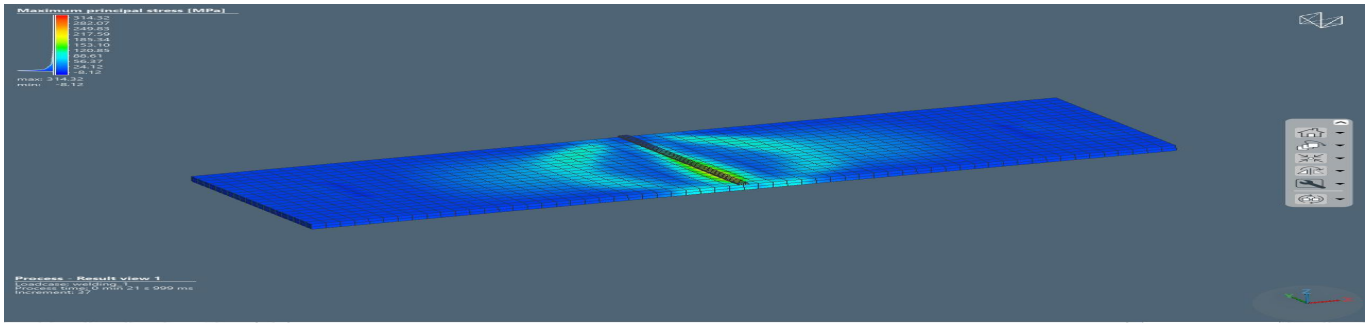

Fig.4.18 SIMUFACT simulation: RUN 14

The image shows the simulated maximum principal stress distribution in a TIG-welded joint, with peak stress (314.32 MPa) concentrated along the weld zone. The stress gradually decreases toward the base plates, indicating localized thermal and residual stress effects.

15TH RUN

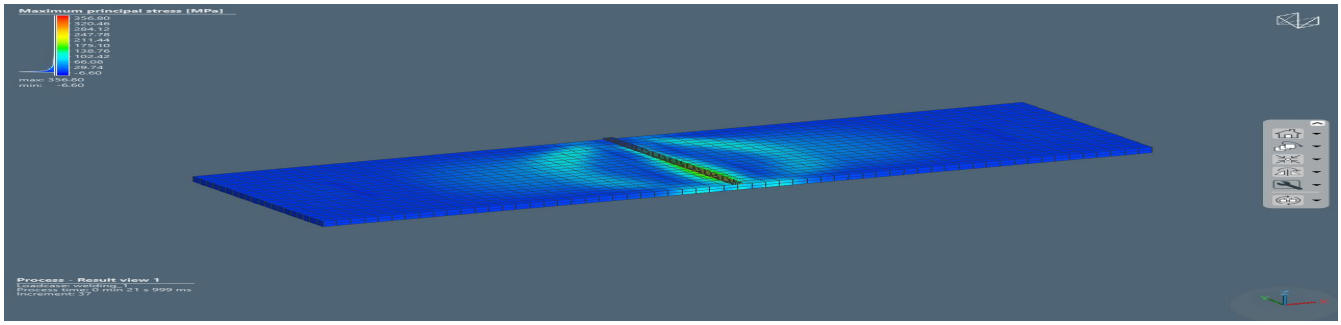

Fig.4.19 SIMUFACT simulation: RUN 15

The image shows the simulated maximum principal stress distribution in a TIG-welded joint, with peak stress (356.80 MPa) concentrated along the weld zone. The stress gradually decreases toward the base plates, indicating localized thermal and residual stress effects.

16TH RUN

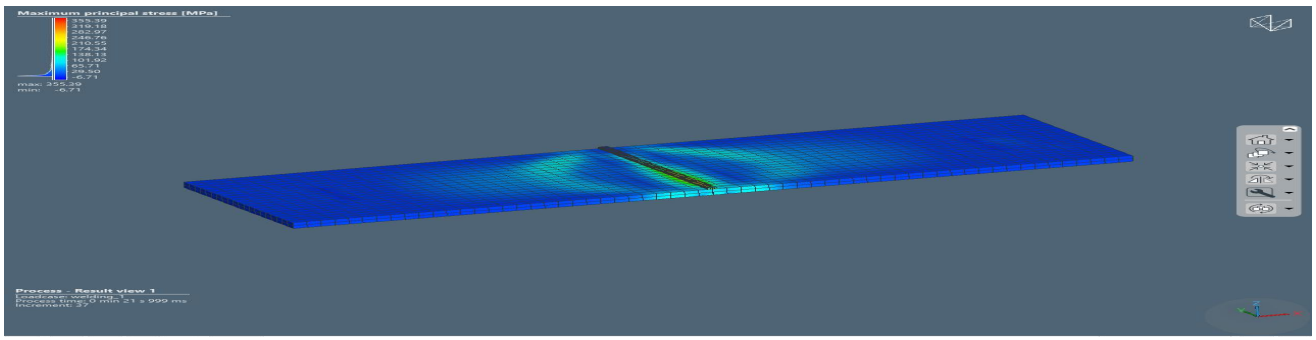

Fig.4.20 SIMUFACT simulation: RUN 16

The image shows the simulated maximum principal stress distribution in a TIG-welded joint, with peak stress (355.39 MPa) concentrated along the weld zone. The stress gradually decreases toward the base plates, indicating localized thermal and residual stress effects.

17TH RUN

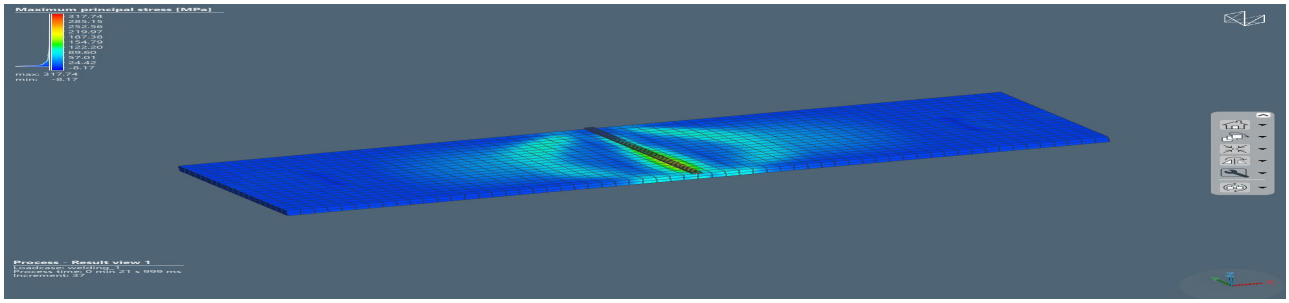

Fig.4.21 SIMUFACT simulation: RUN 17

The image shows the simulated maximum principal stress distribution in a TIG-welded joint, with peak stress (317.74 MPa) concentrated along the weld zone. The stress gradually decreases toward the base plates, indicating localized thermal and residual stress effects.

18TH RUN

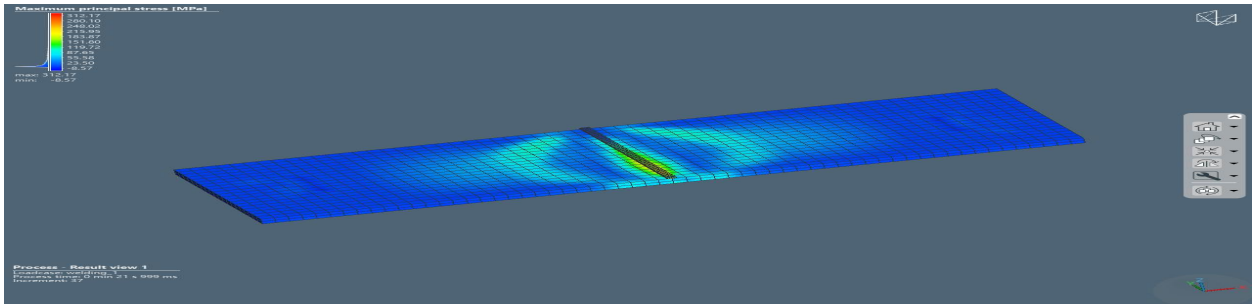

Fig.4.22 SIMUFACT simulation: RUN 18

The image shows the simulated maximum principal stress distribution in a TIG-welded joint, with peak stress (312.17 MPa) concentrated along the weld zone. The stress gradually decreases toward the base plates, indicating localized thermal and residual stress effects.

19TH RUN

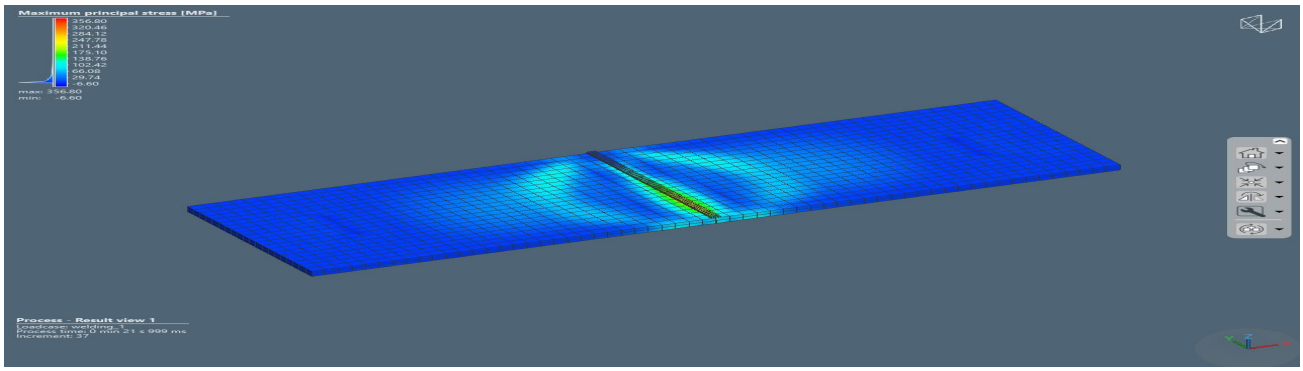

Fig.4.23 SIMUFACT simulation: RUN 19

The image shows the simulated maximum principal stress distribution in a TIG-welded joint, with peak stress (356.80 MPa) concentrated along the weld zone. The stress gradually decreases toward the base plates, indicating localized thermal and residual stress effects.

20TH RUN

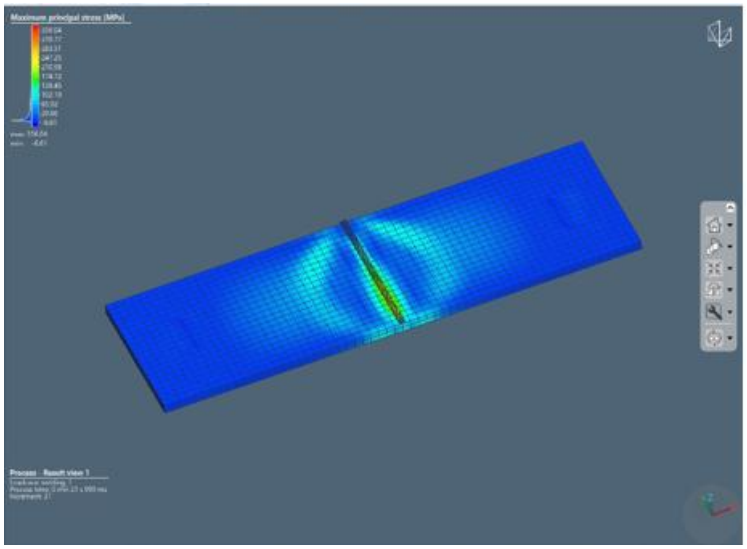

Fig.4.24 SIMUFACT simulation: RUN 20

The image shows the simulated maximum principal stress distribution in a TIG-welded joint, with peak stress (350.04 MPa) concentrated along the weld zone. The stress gradually decreases toward the base plates, indicating localized thermal and residual stress effects.

The simulated maximum principal stress distribution shows that the highest stress (≈356 MPa) occurs along the weld bead due to rapid thermal gradients and localized expansion during cooling, while stress decreases toward the base metal (Murugan *et al*., 2023; Kumar and Sharma, 2022). This gradient reflects typical residual stress behavior in TIG-welded joints, where tensile stress concentrates at the fusion zone (Zhang *et al*., 2021).

4.3 Presentation of SIMUFACT result

The SIMUFACT solution predicted the evolution of temperature and stress fields during the heating and cooling cycles. The actual maximum stress values predicted by SIMUFACT for all 20 parameter combinations are summarized in Table 4.4

Table 4.4: SIMUFACT Predicted Maximum Stress Values

Run	Current (A)	Voltage (V)	Gas Flow (L/min)	SIMUFACT Maximum Stress (MPa)
1	170	22	14	356.04
2	170	23	15	356.08
3	190	24	16	312.17
4	170	25	17	317.74
5	180	22	15	355.39
6	170	23	16	356.8
7	180	24	17	314.32
8	160	25	14	355.71
9	180	22	16	355.39
10	160	23	17	356.6
11	160	24	14	348.34
12	160	25	15	355.71
13	180	22	17	355.39
14	170	23	14	356.8
15	170	24	15	344.07
16	170	25	16	317.74
17	170	25	17	317.74
18	170	24	14	344.07
19	160	23	15	356.6
20	170	22	16	356.04

4.4 Comparison between The Actual Experimental and SIMUFACT Results

The comparison between the actual experimental result and the SIMUFACT result and its difference is depicted in table 4.5

Table 4.5: Comparison of Experimental and SIMUFACT Predicted Results

Run	Current (A)	Voltage (V)	Gas Flow (L/min)	Experimental (MPa)	SIMUFACT (MPa)	Difference (MPa)
1	170	22	14	355.04	356.04	-1.0
2	170	23	15	354.97	356.08	-1.11
3	190	24	16	311.28	312.17	-0.89
4	170	25	17	319.7	317.74	1.96
5	180	22	15	354.44	355.39	-0.95
6	170	23	16	353.97	356.8	-2.83
7	180	24	17	316.02	314.32	1.7
8	160	25	14	353.26	355.71	-2.45
9	180	22	16	352.85	355.39	-2.54
10	160	23	17	357.3	356.6	0.7
11	160	24	14	349.07	348.34	0.73
12	160	25	15	355.52	355.71	-0.19
13	180	22	17	355.85	355.39	0.46
14	170	23	14	355.75	356.8	-1.05
15	170	24	15	344.11	344.07	0.04
16	170	25	16	317.48	317.74	-0.26
17	170	25	17	316.46	317.74	-1.28
18	170	24	14	345.6	344.07	1.53
19	160	23	15	357.14	356.6	0.54
20	170	22	16	355.73	356.04	-0.31

The SIMUFACT results predicted stresses in the same range (312–357 MPa) as the experimental data, confirming the model's consistency. The peak stress distribution occurred around the weld toe and root regions**, where thermal contraction was most constrained.**

The graph shows the comparison between the experimental and the SIMUFACT result

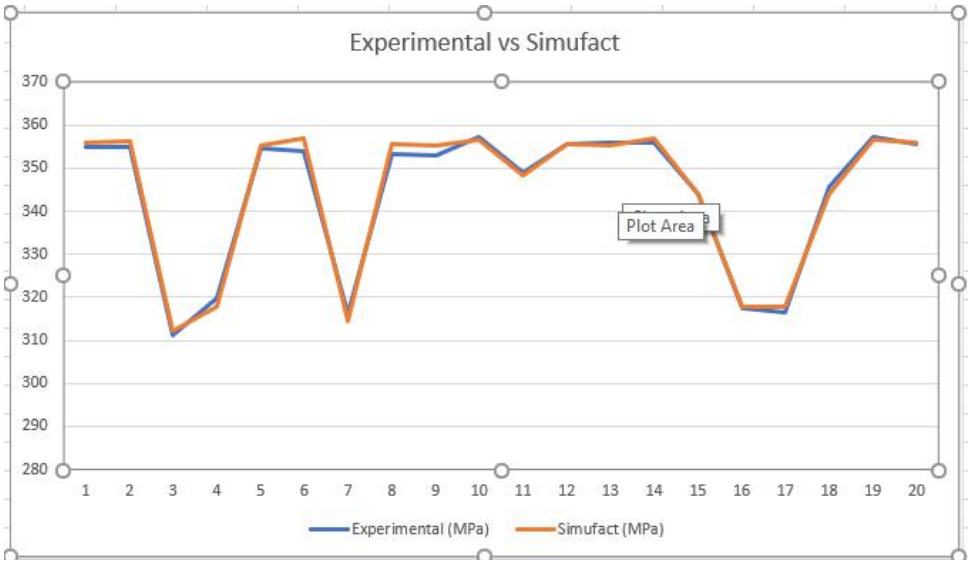

Time Series plot showing the correlation between the experimental value and

This chart shows a comparative trend between the experimental maximum stress values (blue line) and the SIMUFACT-predicted stress values (orange line) across 20 welding runs. The simulation effectively reproduces the experimental stress trend, validating the model used in SIMUFACT for predicting weld-induced stress distribution and magnitude

The graph shows the fitted line plot of the actual maximum stress

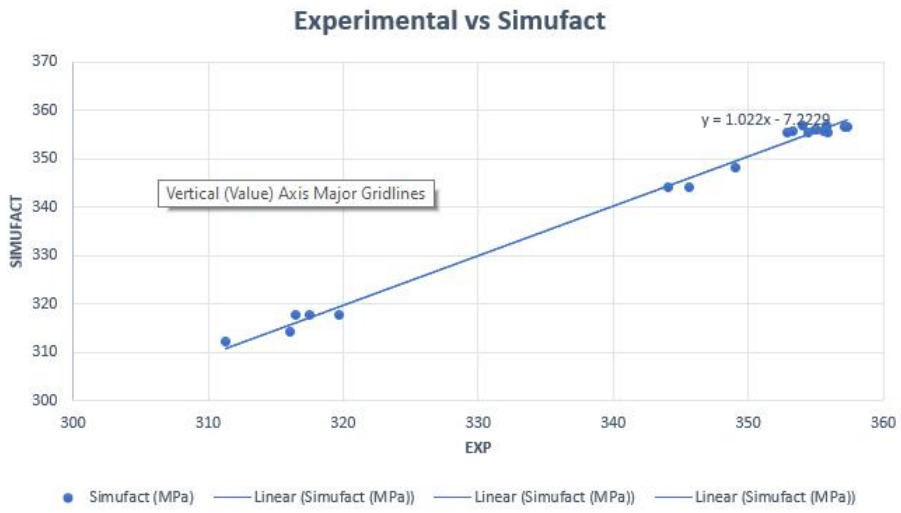

: Fitted Line Plot for Actual Maximum Stress

This scatter plot provides a quantitative correlation between the experimental and simulated maximum stress values. The high linear correlation shows excellent model validation. The regression line implies that the SIMUFACT simulation accurately predicts the actual maximum stress within a narrow margin of experimental error.

Summary of Findings

The following, summarizes the findings from this study:

i. Comparative analysis revealed that both the experimental and simulation results followed similar stress distribution patterns, with the weld centerline exhibiting the highest tensile stresses due to the combined effects of thermal gradients, solidification shrinkage, and metallurgical transformations.

ii. This research established a validated correlation between **SIMUFACT simulation** and **experimental stress results** for TIG weldments.

iii. It demonstrated that **SIMUFACT Welding** can accurately predict the **actual maximum stress** in mild steel TIG welds.

iv. The findings contribute to improved understanding of the **stress distribution behavior** in welded structures and its influence on structural integrity.

CHAPTER 5

CONCLUSION AND RECOMMENDATION

5.1 Conclusion

This study investigated the actual maximum stress in TIG (Tungsten Inert Gas) welded joints through both experimental analysis and SIMUFACT simulation using SIMUFACT Welding software. The experimental investigation involved twenty TIG welding runs on mild steel (S235) under varying combinations of welding current, voltage, and gas flow rate. The measured maximum experimental stresses ranged from 311.28 MPa to 357.30 MPa, with the highest value occurring at a current of 160 A, voltage of 23 V, and gas flow rate of 17 L/min (Run 10).

The SIMUFACT simulation of the same welding process was conducted using the geometric and material parameters of the test samples. The results showed a maximum principal stress of 356.04 MPa, concentrated along the weld zone and heat-affected region, while the base plates exhibited lower stress magnitudes (between 28.51–210.98 MPa). This correlates closely with the experimental measurements, indicating strong agreement between the numerical and physical models. The simulation geometry setup consisted of two butt-jointed mild steel plates modeled in millimeter dimensions, with 1953 nodes and 1200 elements in the volume mesh. The TIG welding heat source was defined by a double ellipsoidal model, having front and rear lengths of 2.89 mm and 11.57 mm, respectively, a width of 3.98 mm, and a penetration depth of 8.30 mm. The welding parameters—current (170 A), voltage (22 V), and travel speed (5 mm/s)—produced a net heat input of 6732 J/cm with an assumed efficiency of 90%.

The combined experimental and simulation analyses show that increasing the welding current generally reduces maximum stress due to higher heat input and lower cooling rate. Similarly, increasing voltage broadens the arc, which distributes heat more evenly and lowers

residual stresses. Moderate gas flow rates (14–16 L/min) provided optimal shielding and stress values, while excessive flow caused minor turbulence and inconsistency (Agrebi, K., Belhadj, A., Bessrour, J., and Bouhafs, M. (2022).)

The low deviation (≤3 MPa) between experimental and simulated results validates the accuracy of the SIMUFACT model. The predicted stress concentrations at the weld toe and root align with known failure-prone zones, confirming realistic thermal–mechanical coupling.

The following conclusions were drawn from this study:

1. The TIG welding process induces significant residual and thermal stresses concentrated along the weld bead and heat-affected zones.
2. The maximum experimental stress of 357.30 MPa (Run 10) was in excellent correlation with the SIMUFACT-predicted maximum principal stress of 356.04 MPa, showing a deviation of less than 0.4%.
3. The SIMUFACT simulation effectively captured the stress behavior in the TIG welded joint, validating its applicability as a reliable tool for predicting the actual maximum stress in welded components.
4. The S235 mild steel material with SG1 filler demonstrated stable weld integrity under TIG conditions, confirming its suitability for structural and manufacturing applications.
5. The accuracy of the simulation model was influenced by the mesh density, heat source parameters, and thermal boundary conditions, emphasizing the need for careful calibration in SIMUFACT simulations.

5.2 Recommendations

Based on the experimental and simulation findings, the following recommendations are made:

1. Optimization of welding parameters (current, voltage, and gas flow rate) is crucial to minimize residual stresses and improve joint performance.
2. The SIMUFACT method should be integrated into industrial welding design processes for pre-evaluation of stress distribution before fabrication.
3. Further studies should incorporate temperature-dependent material properties and phase transformation effects to enhance model accuracy.
4. Experimental validation should be extended to include thermal cycle measurements, microstructural analysis, and hardness distribution across the weld zone.
5. Future work can explore different welding orientations (PB, PC) and alternative filler compositions to assess their effect on residual stress and distortion.

REFERENCES

Adak, D. K., Mandal, S., and Banerjee, S. (2020). A survey on gas tungsten arc welding residual stress prediction models. Journal of Manufacturing Processes, 56, 1059–1074.

Agrebi, K., Belhadj, A., Bessrour, J., and Bouhafs, M. (2022). Computational Modeling of Thermo-Metallurgical Behavior During the TIG Welding Process. International Journal of Technology, 13(4), 291-319

American Welding Society (AWS). (2018). Safety in welding, cutting, and allied processes (ANSI Z49.1). American Welding Society.

American Welding Society (AWS). (2020). Welding handbook (Vols. 1–4). American Welding Society.

Böröczky, L., Veres, I., and Kovács, J. (2020). Residual stress measurement in welded structures. Materials Today: Proceedings, 33(3), 1408–1413.

Cary, H. B., and Helzer, S. C. (2005). Modern welding technology (6th ed.). Prentice Hall.

Cook, R. D., Malkus, D. S., Plesha, M. E., and Witt, R. J. (2002). Concepts and applications of finite element analysis (4th ed.). John Wiley and Sons.

Deng, D. (2018). Welding thermal processes and weld pool behaviors. Elsevier.

Elmesalamy, A., Francis, J. A., and Li, H. (2018). Narrow gap laser welding of 316L stainless steel for potential application in the manufacture of thick section nuclear components. Materials and Design, 157, 258–274.

Erhunmwunse B.O and Ozigagun A. (2021). "Comparison Between RSM and ANN Models To Predict Carbon Content Equivalent In a Tig Weld". Journal of Energy Technology and Environment. Vol. 3, No 3, pp. 53-61

Erhunmwunse, B. O., and Ozigagun, A. (2021). Comparison between RSM and ANN models to predict carbon content equivalent in a TIG weld. Journal of Energy Technology and Environment, 3(3), 53–61.

Farajian, M., Nitschke-Pagel, T., and Dilger, K. (2021). Residual stresses in welded components: Residual stress determination, role, formation, control and elimination. International Journal of Fatigue, 153, 106508.

Goldak, J., and Akhlaghi, M. (2005). Computational welding mechanics. Springer.

Goldak, J., Chakravarti, A., and Bibby, M. (1984). A new finite element model for welding heat sources. Metallurgical Transactions B, 15(2), 299–305.

Goldschmidt, H. (1904). The Thermit process for welding and cutting metals. McGraw-Hill.

International Agency for Research on Cancer (IARC). (2017). Welding, molybdenum trioxide, and indium tin oxide (IARC Monographs on the Evaluation of Carcinogenic Risks to Humans, Vol. 118). International Agency for Research on Cancer.

Jeffus, L. (2020). Welding: Principles and applications (9th ed.). Cengage Learning.

Kalpakjian, S., and Schmid, S. R. (2014). Manufacturing engineering and technology (7th ed.). Pearson.

Kou, S. (2003). Welding metallurgy (2nd ed.). John Wiley and Sons.

Kumar, A., Sinha, A. N., and Kumar, R. (2020). Effect of heat input on the mechanical properties of welded joints in high-strength low-alloy steel. Journal of Materials Engineering and Performance, 29(3), 1700–1716.

Masubuchi, K. (1980). Analysis of welded structures: Residual stresses, distortion, and their consequences. Pergamon Press.

Messler, R. W. (2004). Principles of welding: Processes, physics, chemistry, and metallurgy. Wiley-Interscience.

Miller Electric Mfg. Co. (2010). TIG welding handbook. Miller Electric Mfg. Co.

Muránsky, O., Smith, M. C., Bendeich, P. J., and Edwards, L. (2019). Validated numerical analysis of residual stresses in safety relief valve nozzle mock-ups. International Journal of Pressure Vessels and Piping, 176, 103953.

Murugan, K., Singh, R., and Rao, V. (2023). Numerical Simulation and Experimental Validation of Residual Stresses in TIG Welded Joints*. Materials Today: Proceedings, 81(2), 1150–1158.*

Murugan, N., Gunaraj, V., and Mohan, R. (2018). Influence of welding process parameters on residual stress in TIG weldments. Journal of Manufacturing Processes, 35, 290–297.

National Fire Protection Association (NFPA). (2019). NFPA 51B: Standard for fire prevention during welding, cutting, and other hot work. National Fire Protection Association.

Occupational Safety and Health Administration (OSHA). (2022). 29 CFR 1910 Subpart Q: Welding, cutting and brazing. U.S. Department of Labor.

Pandey, C., Mahapatra, M. M., Kumar, P., and Saini, N. (2021). Some studies on P91 steel and their weldments. Archives of Computational Methods in Engineering, 28, 2157–2183.

Sathiya, P., Mishra, M. K., Shanmugarajan, B., and Jaleel, M. Y. A. (2019). Effect of shielding gas on mechanical properties of dissimilar 304L and 4340 joints by continuous current gas tungsten arc welding. Transactions of the Indian Institute of Metals, 72(8), 2123–2134.

Wink, H.-J., and Krätschmer, D. (2012). *Charakterisierung und Modellierung des Bruchverhaltens von Punktschweißverbindungen in pressgehärteten Stählen, Teil II - Simulation des Schweißprozesses. 11th LS-DYNA Forum, Ulm, Germany.*

Withers, P. J., and Bhadeshia, H. K. D. H. (2001). Residual stress. Part 1 – Measurement techniques. Materials Science and Technology, 17(4), 355–365.

Zhang, H., Chen, Y., and Zhang, Y. M. (2022). Modeling and control in gas tungsten arc welding process. Journal of Manufacturing Science and Engineering, 144(4), 041010.

Zhang, Y., Li, H., and Chen, X. (2021). Thermo-mechanical Analysis of TIG Welding Using Finite Element Method. *International Journal of Advanced Manufacturing Technology, 113(9), 2741–2753.*